



Early View

Original research article

Translational predictions of phase 2a first-in-patient efficacy studies for antituberculosis drugs

Jacqueline P. Ernest, Janice Jia Ni Goh, Natasha Strydom, Qianwen Wang, Rob C. van Wijk, Nan Zhang, Amelia Deitchman, Eric Nuermberger, Rada M. Savic

Please cite this article as: Ernest JP, Goh JJN, Strydom N, *et al.* Translational predictions of phase 2a first-in-patient efficacy studies for antituberculosis drugs. *Eur Respir J* 2023; in press (<https://doi.org/10.1183/13993003.00165-2023>).

This manuscript has recently been accepted for publication in the *European Respiratory Journal*. It is published here in its accepted form prior to copyediting and typesetting by our production team. After these production processes are complete and the authors have approved the resulting proofs, the article will move to the latest issue of the ERJ online.

Translational predictions of phase 2a first-in-patient efficacy studies for antituberculosis drugs

Authors: Jacqueline P. Ernest^{1†}, Janice Jia Ni Goh^{1†}, Natasha Strydom^{1†}, Qianwen Wang^{1†}, Rob C. van Wijk^{1†}, Nan Zhang^{1†}, Amelia Deitchman¹, Eric Nuermberger², Rada M. Savic^{1*}

Affiliation:

¹Department of Bioengineering and Therapeutic Sciences, University of California, San Francisco, San Francisco, California, United States of America

²Center for Tuberculosis Research, Department of Medicine, Johns Hopkins University School of Medicine, Baltimore, Maryland, United States of America

[†]Shared authorship ordered alphabetically

*Corresponding author, E-mail address: rada.savic@ucsf.edu

Address:

1700 4th St, Rm 503C

University of California, San Francisco Box 2552

San Francisco, CA 94158, United States

Telephone number: +1 415 502-0640

E-mail address: rada.savic@ucsf.edu

Running title: Translational pharmacology platform to predict EBA

Abstract

Background: Phase 2a trials in tuberculosis typically use early bactericidal activity (EBA), the decline in sputum colony forming units (CFU) over 14 days, as the primary endpoint for testing the efficacy of drugs as monotherapy. However, the cost of phase 2a trials can range from 7 to 19.6 million dollars on average, while more than 30% of drugs fail to progress to phase 3. Better utilizing preclinical data to predict and prioritize the most likely drugs to succeed will thus help accelerate drug development and reduce costs. We aim to predict clinical EBA using preclinical in vivo pharmacokinetic-pharmacodynamic (PKPD) data and a model-based translational pharmacology approach.

Methods and Findings: First, mouse PK, PD and clinical PK models were compiled. Second, mouse PKPD models were built to derive an exposure response relationship. Third, translational prediction of clinical EBA studies was performed using mouse PKPD relationships and informed by clinical PK models and species-specific protein binding. Presence or absence of clinical efficacy was accurately predicted from the mouse model. Predicted daily decreases of CFU in the first 2 days of treatment and between day 2 and day 14 were consistent with clinical observations.

Conclusion: This platform provides an innovative solution to inform or even replace phase 2a EBA trials, to bridge the gap between mouse efficacy studies and phase 2b and phase 3 trials, and to substantially accelerate drug development.

Introduction

Mycobacterium tuberculosis remains one of the deadliest infectious agents globally. Tuberculosis (TB) drug discovery and development activity has increased emphasis on shorter, more universal regimens to treat all TB cases independent of resistance status¹. However, with an increasing number of new drugs and limited resources for clinical trials, further innovation of drug development is imperative to identify effective drugs and regimens more efficiently and with higher confidence¹. A phase 2a early bactericidal activity (EBA) study is typically the first clinical evaluation of novel anti-TB drug efficacy with the primary purpose of detecting the presence and magnitude of EBA and informing possible dose-response relationships². However, the cost of phase 2a trials can range from 7 to 19.6 million dollars on average, while more than 30% of drugs fail to progress to phase 3³. This highlights the challenges inherent in translating results in preclinical models such as *in vivo* mouse models or *in vitro* hollow-fiber systems, into successful clinical endpoints and outcomes. FDA guidance for industry on drug development for pulmonary TB states appropriate animal models can serve as an important bridge between the identification of *in vitro* antimycobacterial effects of an investigational drug and the initiation of clinical trials⁴. However, traditional translation of findings from preclinical *in vivo* models, by pharmacokinetic modeling and allometric scaling to identify the dosing regimen in humans that best matches the efficacious drug exposure in animals, is insufficient as it only covers exposure, but not response. Mechanistic mouse-to-human pharmacokinetic-pharmacodynamic (PKPD) models that describe the bacterial kill and PKPD relationships are better at predicting clinical results, including the results of late-stage trials⁵. Therefore, our objective is to establish a relevant and robust model-based translational platform that can reliably link preclinical to clinical drug development and

predict early efficacy trials for anti-TB drugs across different compound classes (Figure 1). We compiled a comprehensive preclinical and clinical database of PK, PD, and baseline bacterial growth data for ten drugs. The drugs used to develop and validate our proposed platform consisted of a bacteriostatic antibiotic, namely ethambutol (EMB); five bactericidal antibiotics, namely isoniazid (INH), delamanid (DLM), pretomanid (PMD), linezolid (LZD), and moxifloxacin (MXF); and four sterilizing antibiotics namely rifampin (RIF), rifapentine (RPT), pyrazinamide (PZA), and bedaquiline (BDQ). The translational platform in the present study intends to increase the accuracy of preclinical to clinical translation by enabling quantitative prediction of clinical studies from preclinical outputs and serves as a foundation for model-informed TB drug discovery and development.

Methods

Drug dataset for model building and validation

To build our model and evaluate its predictive accuracy for clinical EBA, ten first- and second-line anti-TB drugs (BDQ, DLM, EMB, INH, LZD, MXF, PMD, PZA, RIF, RPT) were selected for which mouse PK, mouse PD, human population PK models and human clinical EBA data were available.

Data required to assess preclinical drug efficacy

A large database of PK and PD data in mice for 10 TB drugs with clinical EBA data was collected (Figure 2, Table S1). Most experiments were performed at Johns Hopkins University (JHU), with the exception of DLM for which PK data came both from JHU as well as from literature for one dose level⁶, EMB for which PK data came from literature⁷, and LZD which had data from the Tuberculosis Alliance (TBA). PK experiments in BALB/c mice were dose-ranging (2-10 dose levels), single or multiple oral dosing for up to 8 weeks, with 29-238 observations of plasma concentration per drug. PD experiments in BALB/c mice infected through aerosol delivery were dose-ranging (2-15 dose levels) with treatment durations of 21-70 days, and 55-252 observations of lung CFU counts per drug. Lung CFU counts were measured by plating lung homogenates at designated time points. In the case where DLM mouse PK data showed the unexpected trend of a double peak with a single oral dose (Figure 2a), we confirmed the trend with the data provider, JHU.

Mouse PKPD model development

An integrated mouse PKPD model involving a PK model to describe drug exposure, a bacterial dynamics model to account for the mouse immune system and a PD model describing the combined effect of bacterial dynamics and drug effect was developed for each drug. PK data

were described using one- or two-compartment models with first order absorption with or without delay, and saturable elimination when necessary. The bacterial growth dynamics without treatment was described using our previously published baseline model (Eq. S1)⁸. The baseline model captures the decreased rate of growth over time and attributes the decline to time- and bacteria-dependent immune control over the infection. The drug effect, measured as the log₁₀ CFU drop independent of the immune effect over time, was incorporated using a sigmoidal Emax relationship (Eq. S2). A delay effect (K_{delay}) was included to mouse PKPD models to establish an indirect relationship between plasma drug concentrations and drug effect at the site of action (Eq. S3 & S4). Detailed model development and model diagnostics can be found in the Supplemental materials.

Prediction of the clinical EBA

The PKPD relationship quantified in mice was used to predict the clinical EBA. Drug concentrations in humans were simulated based on clinical population pharmacokinetic models (Table S1) to drive the concentration-effect relationship in the clinical predictions. Where clinical population PK models were unavailable, allometric scaling from mouse PK was used⁹. Protein binding ratios between humans and mice ($f_{u\frac{\text{humans}}{\text{mice}}}$) were used to convert unbound plasma drug concentrations from human to mouse to translate the mouse PKPD relationships (Table S1)^{10–16}.

Clinical predictions for 10 drugs were simulated, with 14 unique studies at several dose levels were used for validation by graphically overlaying simulated EBA from preclinical models with observed EBA from clinical trials. Predictions were done by simulating CFU decline in 1000 virtual patients treated with the same dose as reported in the clinical EBA study. The baseline (Day 0) sputum values used were derived from the mean value for each arm reported in each study, and the variability in baseline bacterial burden between individuals used was the baseline variance

among all clinical studies. The net growth and death of bacteria without treatment was assumed to be zero (Eq. S5). Predictions were reported as the mean and standard deviation of the predicted time course of CFU decline. For drugs where observed data were available, the data were overlayed for visual inspection. Finally, quantitative predictions of commonly reported parameters (change from baseline to Day 2 and from Day 2 to Day 14) were compared to the observed at various dose levels along a line of unity.

Software and Statistical method

Preclinical and clinical PKPD modelling was performed in NONMEM (7.4.3) through PsN (4.8.1.). For LZD preclinical PK, Monolix (5.0.0) was used. Models were developed following numerical and graphical diagnostics, assessing drop in objective function value through the likelihood ratio test and parameter precision, as well as goodness-of-fit plots and visual predictive checks, respectively, in addition to pharmacological relevance. Data transformation and graphical output were performed in R (4.1.3) through the RStudio (2022.02.3) interface using the xpose4 and tidyverse packages.

Results

Large preclinical and clinical PK and PD database of ten TB drugs

We collated a rich longitudinal dataset of mouse PK (plasma concentrations, 1220 data points) and PD data (lung CFU counts, 1550 data points), as well as human population PK models and human PD data (sputum CFU counts) (Table S1). PD experiments were done mostly in mouse infection models infected via aerosol with an inoculum size no less than $3.5 \log_{10}$ CFU/ml and incubation periods of 13-17 days, prior to the start of treatment. Exceptions were EMB and LZD, which had incubation periods of 7 and 5 days, respectively, but had a similar inoculation size of larger than $3.5 \log_{10}$ CFU/ml, and RPT which had an incubation period of 41 days but a lower inoculation size than $3.5 \log_{10}$ CFU/ml.

Human PK data were simulated using published models from literature (Table S1 and Figure 2C). Human PD data with a total of 287 human sputum CFU datapoints originating from Phase 2a trials across 14 different studies ranging from 2 to 14 days were used to validate our Phase 2a EBA predictions.

Preclinical PK and PKPD models adequately described mouse data

The final PK and PKPD model parameter estimates are shown in Table 1. A 2-compartment model with saturated clearance described via the Michaelis-Menten equation best described the mouse plasma concentration data for INH, LZD, PMD, PZA and RIF. BDQ, EMB, and MXF were best described using 2-compartment models with linear elimination, RPT by a 1-compartment model with saturated elimination, and DLM by a 1-compartment model with linear elimination. Visual predictive checks of the final model for both mouse PK and PKPD data showed good fits (Figures S1 & S2). The exposure-response relationships for each drug in mouse infection models

are summarized in Table 1 and Figure S3 and aligned with clinical knowledge of the efficacy of each drug.

Clinical EBA was well predicted by the translational platform

The translational platform predicted clinical EBA in TB patients receiving monotherapy with the ten drugs as shown in Figure 3. Our predictions overlapped well with the observed data across multiple doses and time points for most of the drugs. BDQ and LZD had slight over predictions at the later time, and RPT showed activity up to 5 days after a single dose, whereas our model predicted limited declines in CFU.

Agreement between predicted and observed quantitative change in CFU is shown in Figure 4 as a correlation plot for EBA at time intervals of 0-2 days and 2-14 days. Most predictions for 0-2 days fell within $0.25 \log_{10} \text{CFU/ml/day}$ of the observed EBA as indicated by the line of unity and corresponding dotted lines. Predictions for 2-14 days were even closer to observed. Predictions were overall consistent with the observed data in the clinical EBA studies for all ten drugs, except for RPT where activity was underpredicted.

Discussion

We established a mouse-to-human translational platform by integrating a bacterial dynamics model, mouse PKPD relationships, clinical PK and species-specific drug plasma protein binding and validated the platform with clinical EBA data (Figure 1). The changes in sputum CFU counts over the first two days and from Day 2 to Day 14 in TB patients receiving monotherapy with each of ten TB drugs in 14 clinical EBA studies spanning more than four decades were successfully predicted (Figure 3 and 4). Compared to the participants enrolled in more recent EBA studies (2007 to 2015)^{17–23} at the same site, the participants enrolled between 1992 and 2005^{24–28} had more severe disease and therefore higher baseline CFU counts in their sputum samples (mean baseline: $6.9 \log_{10}$ CFU per mL). However, the predictive accuracy of our model was robust despite this large variation in baseline bacterial burden. For example, RIF had a good overlap of predicted and observed EBA (Figure 3) despite the study being conducted in 2015 with the lowest median baseline of $4.58 \log_{10}$ CFU per mL¹⁸.

A key component to our model accuracy was the addition of the bacterial dynamics model. Mouse and human immune activation against TB infection differ significantly, therefore the underlying baseline of bacterial dynamics will differ. Subtracting the mouse immune effect on bacterial decline more accurately estimates the drug contribution to CFU decline. Without such consideration, the clinical CFU decline was overpredicted (Figure S4). Despite inherent differences between species in terms of drug PK, sampling (whole lung homogenate versus sputum), and infecting bacterial strain, the relationship between drug effect on bacteria and the concentration to achieve the effect appear, based on this analysis, to be portable between mice and patients. In addition, although the mouse strain used in the studies (BALB/c) models intracellular bacteria but not extracellular bacteria in caseous lesions²⁹, the PKPD relationships observed in this

model, when derived in comparison to the baseline bacterial dynamics, appear to accurately reflect those observed in EBA studies. Other approaches or more information may be needed to fully account for drug exposures at the site of infection in cavities or other caseous lesions or any PK/PD relationships unique to those microenvironments.

Murine TB models are routinely and often exclusively used as *in vivo* efficacy models in preclinical TB drug development¹. As the inoculum size and incubation period for bacterial infection in the lung prior to treatment can affect drug response⁸, we standardized our inclusion criteria to experiments using the most common design with the incubation duration of 13-17 days and inoculum size to larger than $3.5 \log_{10}$ CFU/ml. Incubation durations outside this range were considered only when data were otherwise not available, which was the case for EMB, LZD and RPT.

Clinical EBA studies are the only acceptable way to evaluate a drug as monotherapy in TB patients despite their limitations on predicting long-term efficacy. In addition to detecting the presence of an EBA response, the trial can inform on the dose-response curve (e.g., INH and RIF), which could be used in dose selection for future trials^{18,30,31}. We have shown here that our translational platform can adequately predict these EBAs for different doses. With limited resources, this costly clinical study can be designed more efficiently or avoided altogether by using our approach to predict a reliable result regarding clinical dose-response effects, and to provide useful information about dose and/or drug candidate selection for further clinical development. This scenario is well exemplified by the nitroimidazole, PMD. PMD has a dose response at doses up to 192 mg/kg in mice which, following the conventional allometric scaling method, approximates 1500 mg in humans. However, such translation is problematic as the clinical observations from two human EBA trials demonstrated no dose response above 200 mg in human

EBA. Using our translational platform, we found that the drug effect of PMD reaches plateau after 200 mg which is consistent with clinical observations (Figure S3). Therefore, our translational platform could serve as a powerful tool for, but not limited to, better dose selection for clinical trials design. By better informing dose selection, the translational modeling platform may reduce the time and effort spent in early clinical development, and therefore, accelerate progress to trials that are more informative of long-term outcomes.

Phase 2a trials also gather information on initial safety and tolerability of compounds of interest which our translational framework is not designed to predict. However, when anti-TB drug development progresses directly to regimen efficacy studies, these safety data can already be captured during Phase 1 healthy volunteer monotherapy studies, especially the multiple ascending dose (MAD) study which is a dose ranging study for up to 4 weeks. The trial population of healthy volunteers is different from the patient population, but safety signals are more pronounced in this healthy population that is more sensitive to adverse events and less burdened by other symptoms. Treatment of healthy volunteers with rifapentine for example resulted in safety signals, but has been proven safe in patients with tuberculosis³². Furthermore, we can also get guidance on the optimal efficacious dose versus the safety range using the dose response curve by overlaying both exposures (Figure S3). All our studied drugs have been previously approved and are used clinically. Having all clinical dose exposures lower than safety limits were thus unsurprising and reassuring. Such dose response curves as visualization would be helpful for determining the dose of new TB drugs too as it provides a measure of both efficacy and safety.

Of the clinical EBA studies included in our analysis, the RPT EBA trial was the only one in which EBA was assessed for multiple days after a single dose. Our human population PK model indicated RPT was mostly cleared from the body two days after a single dose, but the trial results

indicated RPT was still exerting an effect on bacterial load between two and five days post-dose. It is possible that RPT has a post-antibiotic effect that was not sufficiently captured by the model. The model overpredicted the EBA of BDQ. However, in the model, the active metabolite, BDQ-M2, was not considered. In mice, M2 is estimated to contribute approximately 50 percent of the drug effect. One possible reason for the overprediction are the parent-to-metabolite ratios between species that differ, where mice have higher M2-to-BDQ ratios than humans³³. Future studies can account for these differences.

Our translational framework has been developed to predict clinical EBA in the typical adult patient population participating in EBA trials. Heterogeneity in the patient population is an important consideration in drug development and individualized medicine³⁴. This is both from the perspective of representing patients in easy- or hard-to-treat phenotypes as we have observed in our clinical projects as a result from different risk factors (baseline bacterial burden, disease phenotype such as cavitation, gender, comorbidities or comedications), as well as from a diversity perspective to study pharmacology in underrepresented individuals^{35,36}. Certain risk factors such as baseline bacterial burden are easily implementable in our clinical simulations, as well as for example the influence of comorbidities or comedications on the pharmacokinetics. However, preclinical (mouse) models are traditionally more homogeneous to reduce noise in the data and be more sensitive to detect pharmacological signals. At the same time, the EBA trials with relatively small sample sizes (<15 per arm) will also not reflect clinical heterogeneity, and risk factors other than those described above have limited relevance for the prediction of the EBA (e.g. cavitation). Similar considerations are applicable to the prediction of EBA in children. Throughout their development, infants and children show changes in their pharmacology that are well established and can be incorporated in our quantitative model-based framework. Pharmacodynamically, the

bacterial dynamics and the disease phenotype differences can be modelled based on different animal disease models. Children with tuberculosis younger than 1 year have limited immunity which can be approximated through the immunocompromised athymic (nude) mouse model, while dose older than 1 year without lesion phenotypes can be approximated through the BALB/c mouse model. One limitation of these preclinical models is their reliance of bacterial load measurement, which is complicated in the pediatric population in the context of sputum collection. Alternative models are being developed which are part of future collaborative work in our group. Pharmacokinetically, the development of the metabolic pathways responsible for the elimination of anti-tuberculosis drugs can be incorporated through the use of maturation functions. As a result, pediatric dosing can be projected that will reach similar exposure as in adults given a chosen dose, based on the understanding of the maturation of the relevant elimination pathways and the adult pharmacokinetics.

Building on our translational framework, we aim to predict the efficacy of combination regimens of TB drugs in long-term TB clinical outcomes for phase 2b and 3 from preclinical mouse data. Being able to better understand the time to stable culture conversion and relapse 6 months post treatment will better help us prioritize sterilizing regimens. We hope to achieve this by including the characterization of PKPD relationships in combination regimens by accounting for PKPD drug-drug interactions, as well as characterizing lesion-specific PKPD relationships. Technically, the bacterial dynamic parameters of the translational tool will be re-evaluated and possibly updated through Bayesian methods based on untreated control data of ongoing experiments with novel anti-TB drugs, benefiting from a larger data collection while keeping the structure of the translational tool. Clinical TB disease (e.g., caseation necrosis and cavitation) will be represented in the translational platform to include infection and efficacy data in animal models

of TB with more human-like necrotic lesions, such as C3HeB/FeJ mice and New Zealand white rabbits³⁷. This will allow us to have a comprehensive platform that informs us not only of monotherapy EBA but also a combination drug regimens efficacy in providing a stable cure and prevention of long term unfavorable outcomes.

In summary, we established a foundation for translating the results from mouse efficacy models to clinical EBA studies through establishing quantitative relationships involving mouse PK and PD, as well as drug dose response *in vivo*. In the future, our platform will be expanded to include combination regimens and longer durations of treatment by accounting for PKPD drug-drug interactions, and necrotic lesion penetration. This platform is an innovation to accelerate TB drug development and a good example of model-informed drug discovery and development.

Acknowledgements

We acknowledge TB Alliance for support and generously sharing the in-house data of anti-TB drugs linezolid and pretomanid. This work was supported by NIH Grant R01AI-111992.

Author contributions: The manuscript was written by JE, JG, NS, QW, RW, and NZ and commented on by all authors. JE, JG, NS, QW, RW, and NZ contributed to data collection, model development, data and model management, and code review. Contributions to data collection and model development were as follows, JE: BDQ and RPT; JG: EMB; NS: LZD; QW: DLM, PMD, and MXF; NZ: PZA, RIF, and INH. JG and RW revised the manuscript, including generation of figures and tables. JE and RW carried out code review for all drugs. AD worked on data collection, human PK model development, simulation, and preliminary model development. EN provided preclinical data used in our current study, provided substantial scientific context, and edited the manuscript. RS supervised the whole research.

Figures:

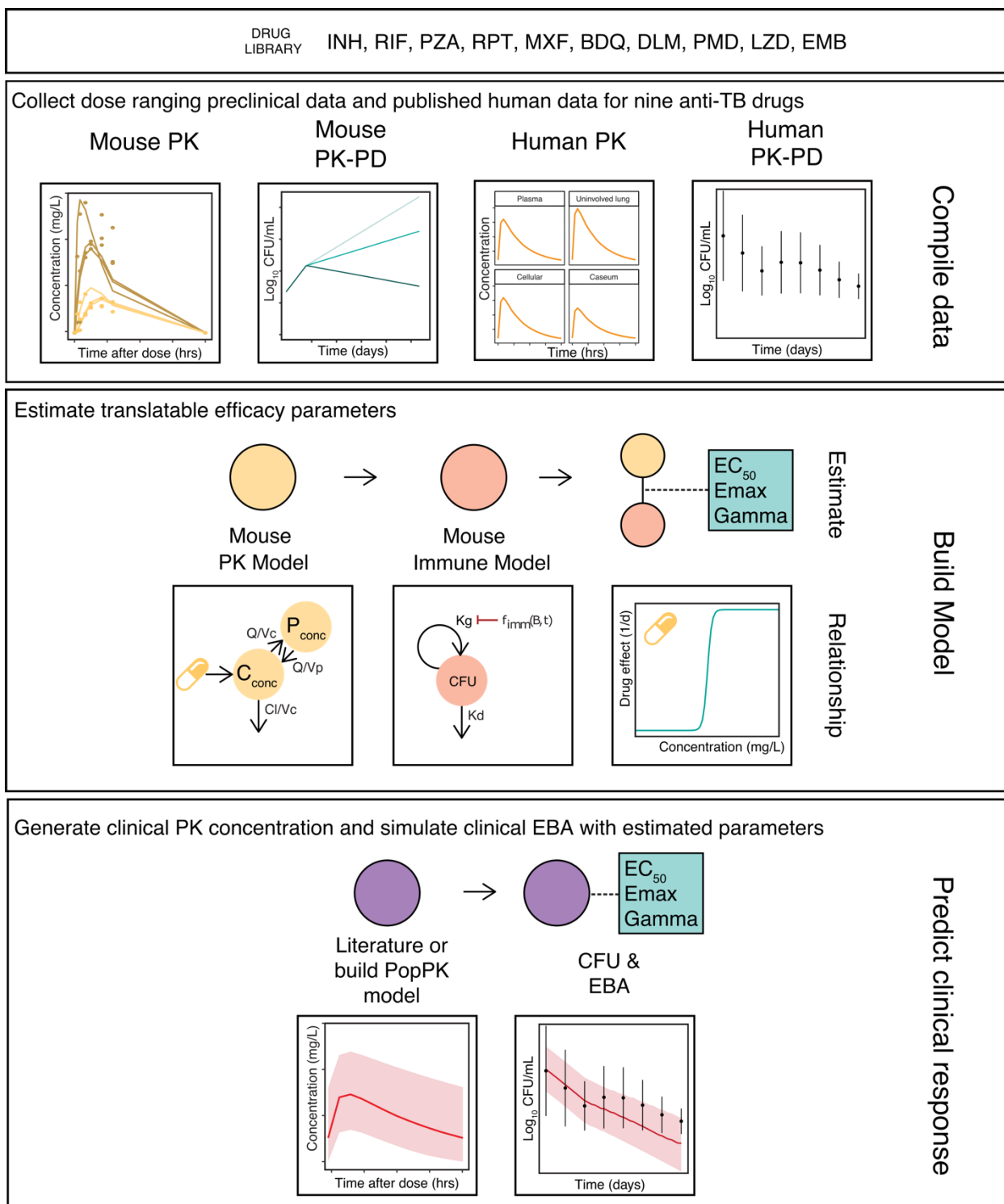


Figure 1. The translational pharmacology approach to predicting early bactericidal activity

in patients. Components necessary for translation include mouse PKPD and clinical PK (actual

or scaled). The estimated relationship between drug concentration and bacterial kill is assumed to be portable after correction for protein binding and integrated with clinical PK. Using baseline bacterial burden from previous EBA trials as initial conditions, the early bactericidal activity is simulated with the translational model.

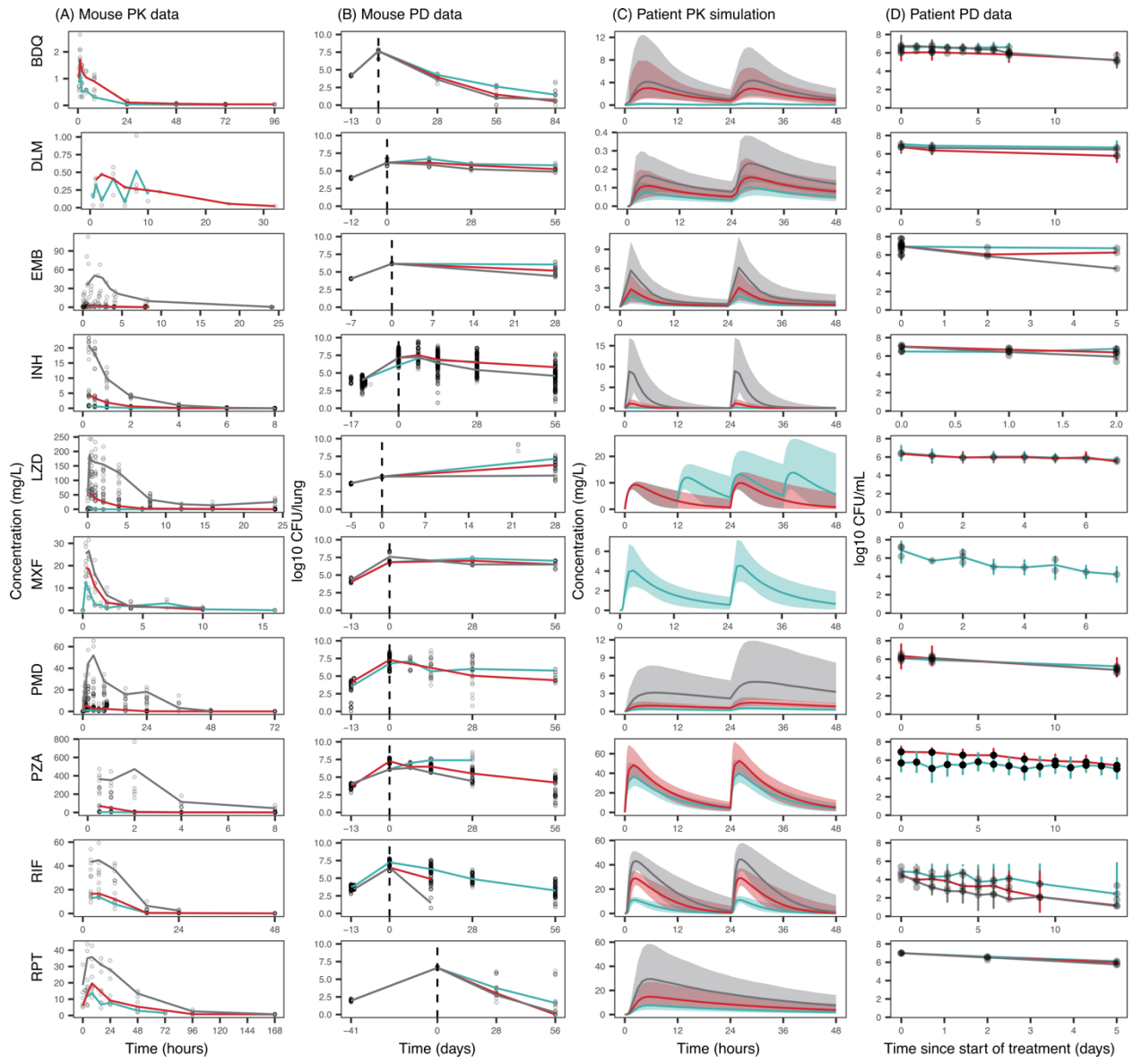


Figure 2. A rich dataset of mouse and human PK and PD data for 10 first- and second-line TB drugs was compiled for model building. Only minimum (blue), median (red) and maximum (grey) doses are represented as median lines when multiple doses were present. Data points for all doses are plotted. Information on all doses is present in Table S1.

(A) Mouse pharmacokinetic (PK) data presented for the following doses: BDQ 12.5, 25 mg/kg; DLM 2.5, 3 mg/kg; EMB 10, 30, 1000 mg/kg; INH 1.56, 6.25, 25 mg/kg; LZD 5, 100, 500 mg/kg; MXF 100, 200, 400 mg/kg; PMD 6, 28.8, 486 mg/kg; PZA 7, 100, 900

mg/kg; RIF 10, 15, 40 mg/kg; RPT 5, 10, 20 mg/kg. All doses were given once daily unless otherwise stated.

- (B) Mouse pharmacodynamic (PD) data presented for the following doses: BDQ 12.5, 25, 50 mg/kg; DLM 3, 10, 100 mg/kg; EMB 100, 400, 1600 mg/kg; INH 0.1, 6.25, 100 mg/kg; LZD 100, 300, 1000 mg/kg; MXF 25, 50, 100 mg/kg; PMD 50, 100 mg/kg; PZA 3, 50, 900 mg/kg; RIF 2.5, 40, 640 mg/kg; RPT 5, 10, 20 mg/kg. All doses were given once daily, 5 days a week, unless otherwise stated.
- (C) Human PK simulations from validated population PK models presented for the following doses: BDQ 25, 200, 400 mg; DLM 100, 200, 400 mg; EMB 15, 25, 50 mg/kg; INH 9, 75, 600 mg; LZD 600 mg once daily, 600 mg twice daily; MXF 400 mg; PMD 50, 200, 1200 mg; PZA 1500, 2000 mg; RIF 600, 1350, 1950 mg; RPT 300, 600, 1200 mg. All doses were given once daily, unless otherwise stated.
- (D) Human Phase 2a early bactericidal activity study data presented for the following doses: BDQ 25, 200, 400 mg; DLM 100, 200, 400 mg; EMB 15, 25, 50 mg/kg; INH 9, 75, 600 mg; LZD 600 mg once daily, 600 mg twice daily; MXF 400 mg; PMD 50, 200, 1200 mg; PZA 200 mg; RIF 600, 1350, 1950 mg; RPT 300, 600, 900, 1200 mg. All doses were given once daily, unless otherwise stated.

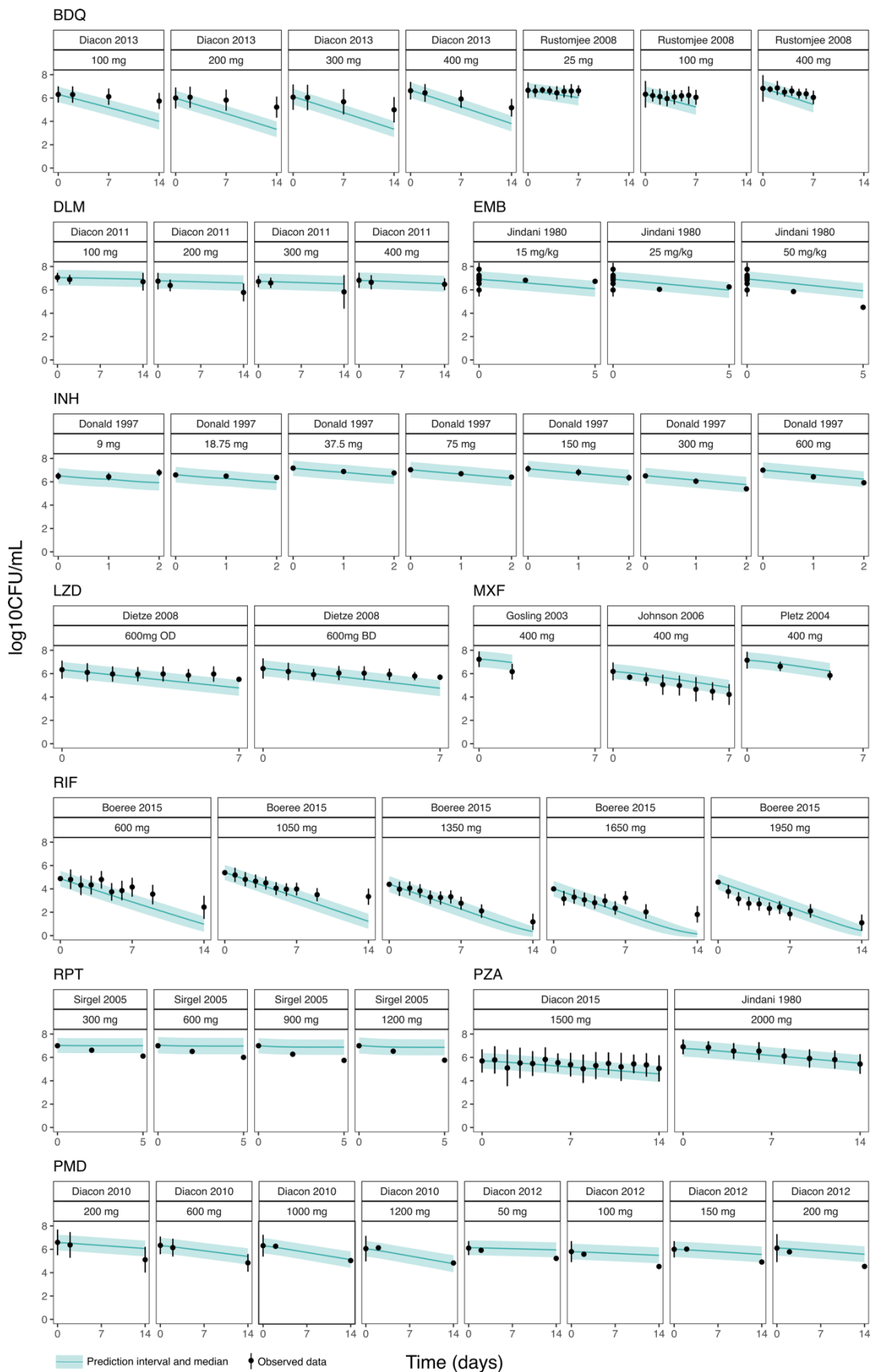


Figure 3. Translational (mouse to human) PKPD model predicts clinical EBA trial results well. Medians and 95% confidence intervals of 1000 simulations from the translational model overlap with observed EBA data from clinical trials.

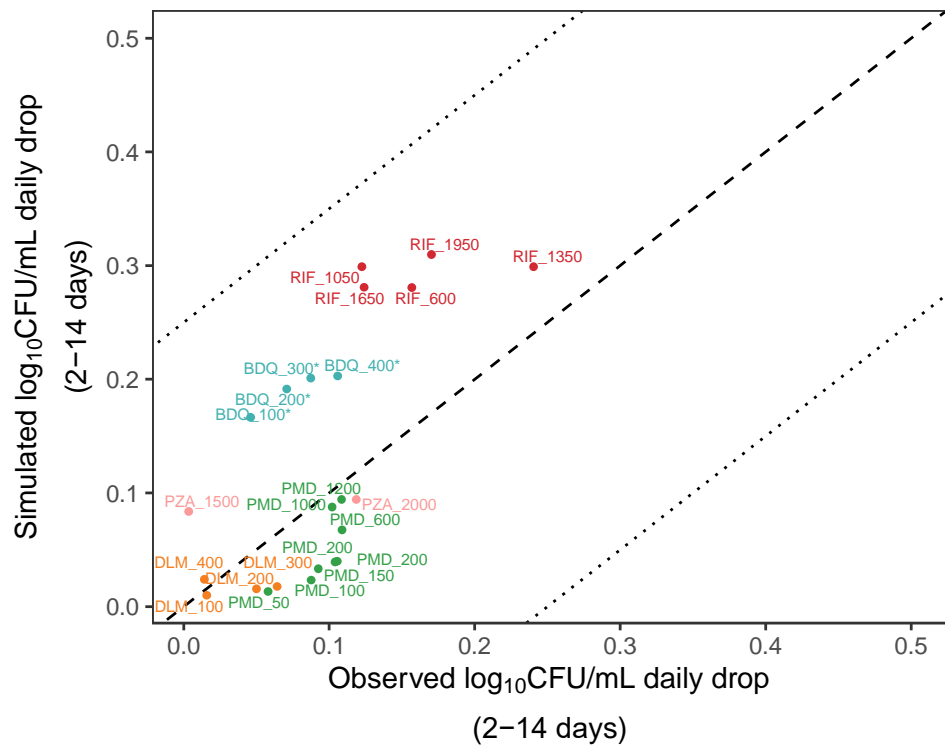
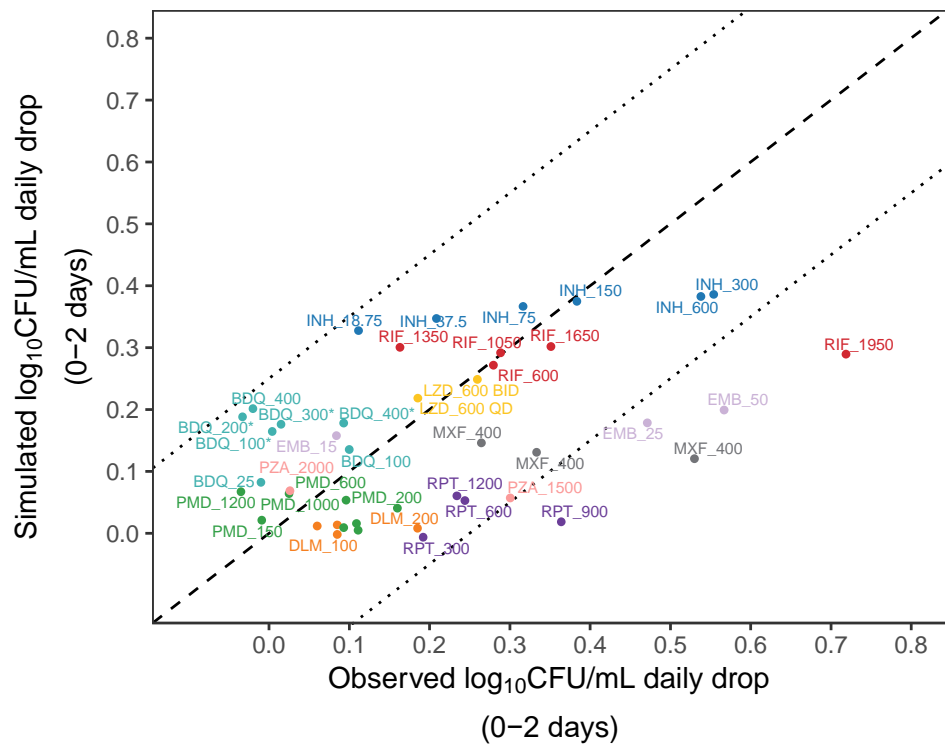


Figure 4. Model-based prediction of daily change in \log_{10} CFU/mL correlates well with clinically observed daily change in \log_{10} CFU/mL for ten TB drugs at multiple dose levels of monotherapy between Day 0 to 2 (top) and Day 2 to 14 (bottom). For some drugs, Day 14 data were not available. Line of unity (dashed line) ± 0.25 (dotted lines). BDQ = bedaquiline, DLM = delamanid, EMB = ethambutol, INH = isoniazid, LZD = linezolid, MXF = moxifloxacin, PMD = pretomanid, PZA = pyrazinamide, RIF = rifampin, RPT = rifapentine. *regimen contained a loading dose

Table 1. Parameter estimates of final PK models for ten TB drugs in mouse studies

Drug	Structural PK model	PK parameters (RSE)	Protein binding ratio (fu, human/mouse)
BDQ	2 compartment, linear elimination	$K_a = 3.24$ (15.1%) h^{-1} $CL = 0.0243$ (5.9%) L/h $V_c = 0.24$ (11.4%) L $V_p = 0.822$ (29.3%) L $Q = 0.0127$ (11.5%) L/h	1.0 ³⁸
DLM	1 compartment, linear elimination	$K_a = 0.446$ h^{-1} (25%) $CL = 0.0092$ L/h (8%) $V_c = 0.0747$ L (1%) $F_{3mg/kg} = 0.758$ (5%)	1.0 ³⁹
EMB ⁷	2 compartment, linear elimination	$CL = 0.0512$ (5.9%) L/h $V_c = 0.0436$ (12.8%) L $V_p = 0.0982$ (7.6%) L $K_a = 0.869$ (9.9%) h^{-1} $Q = 0.0352$ (13.5%) L/h $F = 0.64$ (6.7%) $A_{LAG} = 0.0577$ (11.1) h	1.0
INH	2 compartment, saturated elimination	$CL_{INT} = 31.5$ (8.1%) mL/hr $K_m = 13.1$ (23.2%) $\mu g/mL$ $K_a = 7.89$ (89.4%) $1/hr$ $V_c = 18.6$ (45.0%) mL $Q = 13.3$ (97.7%) mL/hr $V_p = 9.77$ (66.4%) mL	1.455 ^{40,41}
LZD	2 compartment, saturated elimination	$ka = 10 h^{-1}$ FIX $CL_{INT} = 0.0526$ L/h $V_c = 0.0178$ L $V_p = 0.00836$ L $Q = 0.00175$ L/h $K_m = 8.03$ mg/L	0.986 ^{13,42}
MXF	2 compartment, linear elimination	$Ka = 0.0723$ h^{-1} (10%) $Q = 0.1269$ L/h (20%) $V_c = 0.09423$ L (7%) $V_p = 0.3504$ L (25%) $CL = 0.119$ L/h (12 %)	0.797 ⁴³
PMD	2 compartment, saturated	$ka = 2.94$ h^{-1} (31%) $CL_{INT} = 0.0392$ L/h (9%) $V_c = 0.158$ L (7%) $V_p = 0.00568$ L (71%) $Q = 0.00009$ L/h (18%)	0.71 ^{40,44}

	elimination and bioavailability	$K_m = 2.74 \text{ mg/L (24\%)}$ $F_{DIF}=1 \text{ FIX}$ $FD50=363 \text{ mg/kg}$ $\gamma=1 \text{ FIX}$	
PZA	2 compartment, saturated elimination and bioavailability	$CL_{INT}=14.4 \text{ (12\%) ug/hr}$ $K_m=82.9 \text{ (61\%) ug/mL}$ $K_a = 100 \text{ FIX 1/hr}$ $V_c=13.3 \text{ (49\%) mL}$ $Q=3.11 \text{ (19\%) mL/hr}$ $V_p =10.9 \text{ (37\%) mL}$ $F_{17 \text{ mg/kg}} = 1 \text{ FIX}$ $FD50 = 18.2 \text{ (23\%) mg*kg}^{-1}$ $F_{DIF} = 0.574 \text{ (34\%)}$	0.925 ⁴⁵
RIF	2 compartment, saturated elimination and bioavailability	$V_{max}=15.2 \text{ (6\%) ug/hr}$ $K_m=1.16 \text{ (20\%) ug/mL}$ $K_a=0.272 \text{ (10\%) 1/hr}$ $V_1=3.39 \text{ (12\%) mL}$ $Q=0.725 \text{ (6\%) mL/hr}$ $V_2=27.4 \text{ (39\%) mL}$ $F_{10 \text{ mg/kg}}=1 \text{ FIX}$ $F_{15 \text{ mg/kg}}=0.743 \text{ (0\%)}$ $F_{20 \text{ mg/kg}}=0.845 \text{ (1\%)}$ $F_{40 \text{ mg/kg}}=0.493 \text{ (2\%)}$	4.545 ^{41,46}
RPT	1 compartment, saturated elimination	$ka = 0.894 \text{ (31\%) h}^{-1}$ $V = 0.0139 \text{ (6\%) L}$ $K_m = 75.8 \text{ (31\%) ug/mL}$ $V_{max} = 0.0333 \text{ (24\%) ug/hr}$	0.422 ^{47,48}

Complete equations for PK models are found in equations S6-12. 1 compartment model indicates that distribution and elimination phases of the drug were almost instantaneous and can be described by a single central compartment. 2 compartment model indicates that distribution and elimination phases of the drug were distinct and can be described by a central compartment and a peripheral compartment.

Linear elimination indicates that elimination pathways were not saturated with higher doses for the tested dose range. Saturated elimination indicates elimination plateaus after a certain dose.

This relationship can be described by a Michaelis-Menten equation using K_m and V_{max} .

K_a = rate of absorption, CL = linear clearance, V_c = central compartment volume, V_p = peripheral compartment volume, Q = flow between central and peripheral compartments, K_m = concentration that produces half the maximum rate of elimination, V_{max} = maximum rate of elimination. F_1 = relative bioavailability of drug to lowest dose, CL_{int} = intrinsic clearance describing saturated elimination, F = the extent of drug absorbed from oral dosing compartment into systemic compartment, F_{DIF} = the maximum difference in bioavailability from 100% (bound between 0% and 100%), FD_{50} = the dose achieving half maximal reduction in bioavailability, A_{LAG} = absorption lag time.

Table 2. Parameter estimates of final PKPD models for ten TB drugs in mouse studies
parameters

Drug	PK/PD Model	PK/PD Model Parameters	Mouse infection model Type
BDQ	Direct Emax Function	$E_{max} = 0.515$ (1%) day $^{-1}$ $EC_{50} = 0.228$ (5%) mg/L	Subacute
DLM	Delayed Emax Function	$E_{max} = 0.248$ (23%) day $^{-1}$ $EC_{50} = 1.02$ (63%) mg/L $K_{delay} = 91.4$ (0.2%) day $^{-1}$	Subacute
EMB	Direct Emax Function	$E_{max} = 0.527$ (2%) day $^{-1}$ $EC_{50} = 0.150$ (17%) mg/L	Acute
INH	Delayed Emax Function	$E_{max} = 0.901$ (7.5%) day $^{-1}$ $EC_{50} = 0.00404$ (55%) mg/L $K_{delay} = 7.51$ (20%) day $^{-1}$	Subacute
LZD	Delayed Sigmoidal Function	$E_{max} = 1$ day $^{-1}$ (FIX) $EC_{50} = 2.77$ (1%) mg/L $\gamma = 0.21$ (3%) $K_{delay} = 6.75$ (0%) day $^{-1}$	Acute
MXF	Delayed Emax Function	$E_{max} = 0.553$ (10%) day $^{-1}$ $EC_{50} = 0.0000586$ (44%) mg/L $K_{delay} = 0.0000708$ (0.07%) day $^{-1}$	Subacute
PMD	Direct Sigmoidal Function	$E_{max} = 0.429$ (0.1%) day $^{-1}$ $EC_{50} = 3.46$ (0.3%) mg/L $\gamma = 0.375$ (1%) day $^{-1}$	Subacute
PZA	Delayed Emax Function	$E_{max} = 0.34$ (10%) day $^{-1}$ EC_{50} (AUC)= 13.6 (42%) mg*day/L $K_{delay} = 0.797$ (0.2%) day $^{-1}$	Subacute
RIF	Delayed Sigmoidal Function	$E_{max} = 0.678$ (16%) day $^{-1}$ $EC_{50} = 1.92$ (39%) mg/L $\gamma = 1.38$ (24%) $K_{delay} = 1.34$ (79%) day $^{-1}$	Subacute
RPT	Direct Sigmoidal Function	$E_{max} = 0.299$ (1%) day $^{-1}$ $EC_{50} = 6.02$ (0%) mg/L $\gamma = 2.36$ (7%)	Chronic

K_{delay} = the delay rate of the plasma concentration associated with drug effect, E_{max} = the maximal level of drug effect, EC_{50} = the delayed concentration that results in half of the maximal

drug effect, γ = the steepness of the relationship between the delayed plasma concentration and drug effect. Equations are in equations S3-4.

Supporting information

Supplemental Methods

Supplemental Results

Figure S1 Visual predictive checks for final mouse PK models at representative doses

Figure S2 Visual predictive checks for final mouse PD models at representative doses

Figure S3 Comparison between human plasma drug concentrations reached at clinical dose levels (light grey), upper limits of drug concentrations within safety ranges (dark grey) and concentration-response relationships for ten TB drugs

Figure S4 The immune component of the model-based translational platform is essential for accurate prediction of early bactericidal activity

Table S1 Mouse and human PK and PD database of ten TB drugs

Table S2 Final parameters for the bacterial infection model for each drug based on the control data.

References

1. Nuermberger, E. L. Preclinical Efficacy Testing of New Drug Candidates. *Microbiol Spectr* **5**, (2017).
2. Jindani, A., Aber, V. R., Edwards, E. A. & Mitchison, D. A. The early bactericidal activity of drugs in patients with pulmonary tuberculosis. *Am. Rev. Respir. Dis.* **121**, 939–949 (1980).
3. Van Norman, G. A. Phase II Trials in Drug Development and Adaptive Trial Design. *JACC Basic Transl Sci* **4**, 428–437 (2019).
4. DRAFT GUIDANCE. Guidance for Industry. <https://www.fda.gov/media/87194/download>.
5. Danhof, M., de Lange, E. C. M., Della Pasqua, O. E., Ploeger, B. A. & Voskuyl, R. A. Mechanism-based pharmacokinetic-pharmacodynamic (PK-PD) modeling in translational drug research. *Trends Pharmacol. Sci.* **29**, 186–191 (2008).
6. Sasahara, K. *et al.* Pharmacokinetics and Metabolism of Delamanid, a Novel Anti-Tuberculosis Drug, in Animals and Humans: Importance of Albumin Metabolism In Vivo. *Drug Metab. Dispos.* **43**, 1267–1276 (2015).
7. Chen, C., Ortega, F., Alameda, L., Ferrer, S. & Simonsson, U. S. H. Population pharmacokinetics, optimised design and sample size determination for rifampicin, isoniazid, ethambutol and pyrazinamide in the mouse. *Eur. J. Pharm. Sci.* **93**, 319–333 (2016).
8. Zhang Nan *et al.* Mechanistic Modeling of Mycobacterium tuberculosis Infection in Murine Models for Drug and Vaccine Efficacy Studies. *Antimicrob. Agents Chemother.* **64**, e01727-19 (2020).
9. U.S. Department of Health and Human Services, Food and Drug Administration, Center for Drug Evaluation and Research (CDER). Guidance for Industry Estimating the Maximum Safe Starting Dose in Initial Clinical Trials for Therapeutics in Adult Healthy Volunteers. Preprint at <https://www.fda.gov/media/72309/download> (2005).

10. Svensson, E. M., Dosne, A.-G. & Karlsson, M. O. Population Pharmacokinetics of Bedaquiline and Metabolite M2 in Patients With Drug-Resistant Tuberculosis: The Effect of Time-Varying Weight and Albumin. *CPT Pharmacometrics Syst Pharmacol* **5**, 682–691 (2016).
11. Patterson, S. *et al.* The anti-tubercular drug delamanid as a potential oral treatment for visceral leishmaniasis. *Elife* **5**, (2016).
12. Alghamdi, W. A., Al-Shaer, M. H. & Peloquin, C. A. Protein Binding of First-Line Antituberculosis Drugs. *Antimicrob. Agents Chemother.* **62**, (2018).
13. Dryden, M. S. Linezolid pharmacokinetics and pharmacodynamics in clinical treatment. *J. Antimicrob. Chemother.* **66**, iv7–iv15 (2011).
14. Dorn, C. *et al.* Decreased protein binding of moxifloxacin in patients with sepsis? *GMS Infect Dis* **5**, Doc03 (2017).
15. Committee for Medicinal Products for Human Use (CHMP). Assessment report Pretomanid FGK International non-proprietary name: pretomanid. Preprint at https://www.ema.europa.eu/en/documents/assessment-report/pretomanid-fgk-epar-public-assessment-report_en.pdf (2020).
16. Egelund, E. F. *et al.* Protein binding of rifapentine and its 25-desacetyl metabolite in patients with pulmonary tuberculosis. *Antimicrob. Agents Chemother.* **58**, 4904–4910 (2014).
17. Diacon, A. H. *et al.* Phase II dose-ranging trial of the early bactericidal activity of PA-824. *Antimicrob. Agents Chemother.* **56**, 3027–3031 (2012).
18. Boeree, M. J. *et al.* A dose-ranging trial to optimize the dose of rifampin in the treatment of tuberculosis. *Am. J. Respir. Crit. Care Med.* **191**, 1058–1065 (2015).
19. Diacon, A. H. *et al.* Early bactericidal activity of delamanid (OPC-67683) in smear-positive pulmonary tuberculosis patients. *Int. J. Tuberc. Lung Dis.* **15**, 949–954 (2011).

20. Rustomjee, R. *et al.* Early bactericidal activity and pharmacokinetics of the diarylquinoline TMC207 in treatment of pulmonary tuberculosis. *Antimicrob. Agents Chemother.* **52**, 2831–2835 (2008).
21. Diacon, A. H. *et al.* Randomized dose-ranging study of the 14-day early bactericidal activity of bedaquiline (TMC207) in patients with sputum microscopy smear-positive pulmonary tuberculosis. *Antimicrob. Agents Chemother.* **57**, 2199–2203 (2013).
22. Dietze, R. *et al.* Early and extended early bactericidal activity of linezolid in pulmonary tuberculosis. *Am. J. Respir. Crit. Care Med.* **178**, 1180–1185 (2008).
23. Diacon, A. H. *et al.* Bactericidal activity of pyrazinamide and clofazimine alone and in combinations with pretomanid and bedaquiline. *Am. J. Respir. Crit. Care Med.* **191**, 943–953 (2015).
24. Donald, P. R. *et al.* The early bactericidal activity of isoniazid related to its dose size in pulmonary tuberculosis. *Am. J. Respir. Crit. Care Med.* **156**, 895–900 (1997).
25. Gosling, R. D. *et al.* The bactericidal activity of moxifloxacin in patients with pulmonary tuberculosis. *Am. J. Respir. Crit. Care Med.* **168**, 1342–1345 (2003).
26. Johnson, J. L. *et al.* Early and extended early bactericidal activity of levofloxacin, gatifloxacin and moxifloxacin in pulmonary tuberculosis. *Int. J. Tuberc. Lung Dis.* **10**, 605–612 (2006).
27. Pletz, M. W. R. *et al.* Early bactericidal activity of moxifloxacin in treatment of pulmonary tuberculosis: a prospective, randomized study. *Antimicrob. Agents Chemother.* **48**, 780–782 (2004).
28. Sirgel, F. A. *et al.* The early bactericidal activities of rifampin and rifapentine in pulmonary tuberculosis. *Am. J. Respir. Crit. Care Med.* **172**, 128–135 (2005).
29. Kramnik, I. & Beamer, G. Mouse models of human TB pathology: roles in the analysis of necrosis and the development of host-directed therapies. *Semin. Immunopathol.* **38**, 221–237 (2016).

30. Diacon, A. H. *et al.* Multidrug-resistant tuberculosis and culture conversion with bedaquiline. *N. Engl. J. Med.* **371**, 723–732 (2014).
31. Donald, P. R. & Diacon, A. H. The early bactericidal activity of anti-tuberculosis drugs: a literature review. *Tuberculosis* **88 Suppl 1**, S75-83 (2008).
32. Dooley, K. E. *et al.* Safety and pharmacokinetics of escalating daily doses of the antituberculosis drug rifapentine in healthy volunteers. *Clin. Pharmacol. Ther.* **91**, 881–888 (2012).
33. Ngwalero, P. *et al.* Relationship between Plasma and Intracellular Concentrations of Bedaquiline and Its M2 Metabolite in South African Patients with Rifampin-Resistant Tuberculosis. *Antimicrob. Agents Chemother.* **65**, e0239920 (2021).
34. Brown, K. *et al.* Diversity in Clinical Pharmacology: A Call to Action. *Clin. Pharmacol. Ther.* **113**, 483–485 (2023).
35. Imperial, M. Z. *et al.* A patient-level pooled analysis of treatment-shortening regimens for drug-susceptible pulmonary tuberculosis. *Nat. Med.* **24**, 1708–1715 (2018).
36. Imperial, M. Z., Phillips, P. P. J., Nahid, P. & Savic, R. M. Precision-Enhancing Risk Stratification Tools for Selecting Optimal Treatment Durations in Tuberculosis Clinical Trials. *Am. J. Respir. Crit. Care Med.* **204**, 1086–1096 (2021).
37. Ernest, J. P. *et al.* Development of New Tuberculosis Drugs: Translation to Regimen Composition for Drug-Sensitive and Multidrug-Resistant Tuberculosis. *Annu. Rev. Pharmacol. Toxicol.* **61**, 495–516 (2021).
38. SIRTURO-pi.pdf.
39. Shimokawa, Y. *et al.* Metabolic Mechanism of Delamanid, a New Anti-Tuberculosis Drug, in Human Plasma. *Drug Metab. Dispos.* **43**, 1277–1283 (2015).
40. Jayaram, R. *et al.* Isoniazid pharmacokinetics-pharmacodynamics in an aerosol infection model of tuberculosis. *Antimicrob. Agents Chemother.* **48**, 2951–2957 (2004).

41. Woo, J. *et al.* In vitro protein binding characteristics of isoniazid, rifampicin, and pyrazinamide to whole plasma, albumin, and alpha-1-acid glycoprotein. *Clin. Biochem.* **29**, 175–177 (1996).
42. Lepak, A. J., Marchillo, K., Pichereau, S., Craig, W. A. & Andes, D. R. Comparative pharmacodynamics of the new oxazolidinone tedizolid phosphate and linezolid in a neutropenic murine *Staphylococcus aureus* pneumonia model. *Antimicrob. Agents Chemother.* **56**, 5916–5922 (2012).
43. Siefert, H. M. *et al.* Pharmacokinetics of the 8-methoxyquinolone, moxifloxacin: a comparison in humans and other mammalian species. *J. Antimicrob. Chemother.* **43 Suppl B**, 69–76 (1999).
44. Rakesh *et al.* Synthesis and evaluation of pretomanid (PA-824) oxazolidinone hybrids. *Bioorg. Med. Chem. Lett.* **26**, 388–391 (2016).
45. Stada Pharmaceuticals, Inc, Cranbury, NJ, 2004. Product Information: pyrazinamide oral tablets, pyrazinamide oral tablets. Preprint at
https://www.micromedexsolutions.com/micromedex2/librarian/CS/E2AC9E/ND_PR/evidenceexpert/ND_P/evidenceexpert/DUPLICATIONSHIELDSYNC/C17097/ND_PG/evidenceexpert/ND_B/evidenceexpert/ND_AppProduct/evidenceexpert/ND_T/evidenceexpert/PFACTIONId/evidenceexpert/ND_DoIntegratedSearch?SearchTerm=pyrazinamide&UserSearchTerm=pyrazinamide&SearchFilter=filterNone&navitem=searchALL#cite5_dp.
46. de Steenwinkel, J. E. M. *et al.* Optimization of the rifampin dosage to improve the therapeutic efficacy in tuberculosis treatment using a murine model. *Am. J. Respir. Crit. Care Med.* **187**, 1127–1134 (2013).
47. sanofi-aventis U.S. (per manufacturer), Bridgewater, NJ, 2014. Product Information: PRIFTIN(R) oral tablets, rifapentine oral tablets. Preprint at
https://www.micromedexsolutions.com/micromedex2/librarian/CS/A32D19/ND_PR/evidenceexpert/ND_P/evidenceexpert/DUPLICATIONSHIELDSYNC/0EBD73/ND_PG/evidenceexpert/ND_B/evidenceexpert/ND_AppProduct/evidenceexpert/ND_T/evidenceexpert/PFACTIONId/evidenceexpert/ND_DoIntegratedSearch?SearchTerm=rifapentine&UserSearchTerm=rifapentine&SearchFilter=filterNone&navitem=searchALL#cite5_dp

- ert.DoIntegratedSearch?SearchTerm=rifapentine&UserSearchTerm=rifapentine&SearchFilter=f
ilterNone&navitem=searchALL#cite2_dp.
48. Assandri, A., Ratti, B. & Cristina, T. Pharmacokinetics of rifapentine, a new long lasting rifamycin, in the rat, the mouse and the rabbit. *J. Antibiot.* **37**, 1066–1075 (1984).

Supplementary Material to:

**Translational predictions of phase 2a first-in-patient efficacy studies
for antituberculosis drugs**

Jacqueline P. Ernest^{1†}, Janice Jia Ni Goh^{1†}, Natasha Strydom^{1†}, Qianwen Wang^{1†},
Rob C. van Wijk^{1†}, Nan Zhang^{1†}, Amelia Deitchman¹, Eric Nuermberger², Rada
M. Savic^{1*}

Affiliation:

¹Department of Bioengineering and Therapeutic Sciences, University of California, San Francisco,
San Francisco, California, United States of America

²Center for Tuberculosis Research, Department of Medicine, Johns Hopkins University School of
Medicine, Baltimore, Maryland, United States of America

[†]Shared authorship ordered alphabetically

*Corresponding author

Address:

1700 4th St, Rm 503C

University of California, San Francisco Box 2552

San Francisco, CA 94158, United States

Telephone number: +1 415 502-0640

E-mail address: rada.savic@ucsf.edu

Supplemental Methods

Study design

This translational platform is designed to understand the PK/PD relationships of TB drugs in murine TB model and extrapolate the findings to predict the clinical outcomes of phase 2a studies (Figure 1). Ten drugs were included: bedaquiline (BDQ), delamanid (DLM), ethambutol (EMB), isoniazid (INH), linezolid (LZD), moxifloxacin (MXF), pretomanid (PMD), pyrazinamide (PZA), rifampin (RIF), and rifapentine (RPT). A baseline model using the preclinical data in murine TB model was established previously to quantitate the inhibitory effect of the adaptive immune response on bacterial growth, and a net drug effect can therefore be quantified to establish the PK/PD relationships for the experimental regimens in mice. It was assumed at the free drug concentration level in blood, the PK/PD relationships of TB drugs are comparable between mice and humans. As such, with simulated PK concentrations in humans, the corresponding drug effect of TB drugs in humans can be predicted using the same PK/PD relationships as in mice, as well as the clinical outcome of TB monotherapy regimens in phase 2a trials.

Database

The sources for all data involved in the translational platform development are listed in **Table S1**. Preclinical plasma PK concentrations and lung CFU counts as PD data of BDQ, DLM, EMB, INH, LZD, MXF, PMD, PZA, RIF and RPT were collected from published and unpublished studies or digitized from published studies using Plot Digitizer (<http://plotdigitizer.sourceforge.net/>). Subacute infection data was used for all drugs except EMB, RPT and LZD for which data from the subacute infection model were not available. Clinical PK data were simulated using published human population PK models or models developed internally.

CFU counts in sputum samples for the nine drugs were collected or digitized from published clinical studies.

Model development

All analyses were conducted using NONMEM (version 7.4). Perl speaks NONMEM (PsN, 4.8.1), R (version 4.1.3) statistical program, and the xpose4 and tidyverse R packages were utilized for model diagnostics and data visualization. The first-order conditional estimation with interaction method (FOCE+I) was used. Mouse PK and PK/PD models were developed and selected based on graphical (goodness of fit plots), statistical (significant change in objective function value), and simulation-based diagnostics (visual predictive checks).

Mouse PK models for all drugs except EMB for which no PK data was available, were developed by fitting the plasma concentration data to one- or two-compartment structural models with first-order absorption and linear or nonlinear (Michaelis-Menten) clearance. Saturable bioavailability was also tested. Additive, proportional, and combination residual error models were tested to describe the error in the observed data (Figure S1). An EMB mouse PK model was utilized from literature to simulate EMB PK¹.

Mouse PK/PD models were developed by incorporating drug effects into a bacterial infection model that describes the infection of *M. tuberculosis* in BALB/c mice (Eq. S1 & Eq. S2). Parameters of the bacterial infection model were re-estimated based on the control data for each drug, to fit the untreated bacterial burden over time for their respective experiment and reliably quantify the drug efficacy separate from the natural infection dynamic (**Table S2**)². The inhibitory effect of the adaptive immune response during the treatment period was investigated with certain assumptions. Plasma concentration was used as the independent variable to describe the treatment response for all mouse PD studies except that of PZA using cumulative AUC in acute and sub-

acute infection model studies due to the time-varying PZA effect being dependent upon the pH of the microenvironment in the phagosomal compartment during the early treatment period which is, itself, a function of the time ($Conc_{PZA} \times dt$).

PK/PD relationships for drug effect were optimized by fitting the log-transformed mouse PD data to linear, nonlinear, log-linear, E_{max} and sigmoidal functions. A delay effect was added to optimize the relationship between plasma exposures, time and treatment response (Eq. S3 & S4, Figure S2). An additive error model was used to describe residual error for the mouse PK/PD models. Visual predictive checks (VPCs) of 1000 simulations indicated that the observed data were consistently within the 95% prediction interval of the simulated plasma concentrations and bacterial numbers in the final PK and PK/PD models used for translation for each drug (Figure S2).

$$\frac{dB}{dt} = K_g \times B \times \left(1 - \frac{K_B \times B^{\gamma_B}}{B_{50}^{\gamma_B} + B^{\gamma_B}}\right) \times \left(1 - \frac{K_T \times t^{\gamma_T}}{T_{50}^{\gamma_T} + t^{\gamma_T}}\right) - K_d \times B \quad Eq. S1$$

$$\frac{dB}{dt} = K_g \times B \times \left(1 - \frac{K_B \times B^{\gamma_B}}{B_{50}^{\gamma_B} + B^{\gamma_B}}\right) \times \left(1 - \frac{K_T \times t^{\gamma_T}}{T_{50}^{\gamma_T} + t^{\gamma_T}}\right) - K_d \times B - EFF \times B \quad Eq. S2$$

B: bacterial number

t: incubation time since inoculation

K_g: bacterial growth rate

K_d: bacterial natural death rate

K_B: bacterial number-dependent maximal adaptive immune effect

B₅₀: bacterial number that results in half of *K_B*

γ_B: steepness of bacterial number-dependent immune effect relationship

K_T: incubation time-dependent maximal adaptive immune effect

T₅₀: bacterial number that results half of *K_T*

γ_T : steepness of time-dependent immune effect relationship

EFF: bacterial killing rate

$$\frac{dA_{\text{delay}}}{dt} = K_{\text{delay}} \times \left(\frac{A_2}{V_1} - A_{\text{delay}} \right) \quad \text{Eq. S3}$$

A_{delay} : the delayed concentration level associated with drug effect

K_{delay} : the delay rate of the plasma concentration associated with drug effect

$$EFF = \frac{A_{\text{delay}}^\gamma \times E_{\text{max}}}{EC_{50}^\gamma + A_{\text{delay}}^\gamma} \quad \text{Eq. S4}$$

E_{max} : the maximal level of drug effect

EC_{50} : the delayed concentration that results in half of the maximal drug effect

γ : the steepness of the relationship between the delayed plasma concentration and drug effect

Clinical PK models were implemented from either published models or developed in NONMEM based on either internal clinical data or extracted literature data (**Table S1**). Single and multi-compartment PK models were tested for drugs modeled. Linear and nonlinear clearance, absorption and bioavailability were also tested when appropriate. Additive, proportional and combination residual error models were tested for the best fit.

Translational model development for EBA prediction

The outcome of clinical EBA studies was predicted by translating the mouse exposure-response relationships to TB patients. Either average patient covariates or no covariates were included for simulating human PK exposures for each drug. The outcomes of EBA studies were predicted by simulating the CFU counts in the sputum of TB patients based on the translatable PK/PD relationships identified in the mouse efficacy studies. Drug dose was as specified in the

EBA publication, where weight-based dosing was multiplied by the median weight in the studied population and rounded based on available formulations. In the untreated control arm, typically minimal changes occur during the first two days of study (1-8). As such, the net CFU count change rate (K_{net}) during the first two days of study was considered to be 0 and the changes in CFU counts were only driven by the drug effect (*Eq. S5*).

$$\frac{dB}{dt} = K_{net} \times B - EFF \times B \quad Eq. S5$$

K_{net}: the net rate of change in bacterial number in the sputum of TB patients

EBA values were calculated as the daily change of CFU counts over specific days with treatment for ten drugs individually. A thousand simulations for predicting clinical studies were conducted for each drug.

Supplemental Results

Mouse PK and PK/PD Model Development

Mouse PK models of nine out of the ten TB drugs, including BDQ, DLM, INH, LZD, MXF, PMD, PZA, RIF and RPT, were developed using plasma concentration data individually, among which partial data for DLM were digitized from a published study (3 mg/kg)³. EMB PK was simulated using a published mouse PK model¹. Either a one-compartment or two-compartment structural model with first-order absorption and linear or non-linear clearance was used to describe the mouse PK data for each drug (Supplementary Figure S1, Table 1) (*Eq. S6-S11*). Saturable bioavailability was incorporated for PMD and RIF PK models (*Eq. S12*).

First-order Absorption model:

$$\frac{dA_1}{dt} = -K_a \times A_1 \quad Eq. S6$$

A_1 is the amount of drug in the gastrointestinal tract absorbed into the systemic circulation

K_a is the first-order absorption rate of the drug

t is the time after the dos

One-compartment PK model:

$$\frac{dA_2}{dt} = K_a \times A_1 - K_e \times A_2 \quad Eq. S7$$

A_2 is the amount of drug in the central compartment

K_e is the elimination rate of the drug from the central compartment

Two-compartment PK model:

$$\frac{dA_2}{dt} = K_a \times A_1 - K_e \times A_2 - \frac{Q}{V_1} \times A_2 + \frac{Q}{V_2} \times A_3 \quad Eq. S8$$

$$\frac{dA_3}{dt} = \frac{Q}{V_1} \times A_2 - \frac{Q}{V_2} \times A_3 \quad Eq. S9$$

A_3 is the amount of drug in the peripheral compartment

Q is the intercompartmental clearance

V_1 is the volume of the central compartment

V_2 is the volume of the peripheral compartment

Linear clearance:

$$K_e = \frac{CL}{V_1} \quad Eq. S10$$

CL is the clearance, which is defined as the volume of plasma completely cleared of a drug per unit time

Non-linear clearance:

$$K_e = \frac{K_m \times CL_{in}}{(K_m + \frac{A_2}{V_1}) \times V_1} \quad Eq. S11$$

V_{max} is the maximal clearance, which is defined as the maximal volume of plasma completely cleared of a drug per unit time

K_m is the concentration of drug that results in half of the maximal clearance

CL_{in} is the ratio between V_{max} and K_m .

Saturable bioavailability:

$$F = 1 - \frac{FD_{IF} \times (Dose - Dose_{ref})}{Dose - Dose_{ref} + FD_{50}} \quad Eq. S12$$

F : the extent of drug absorbed from oral dosing compartment into systemic compartment

FD_{IF} : the maximum difference in bioavailability from 100% (bound between 0% and 100%)

$Dose_{ref}$: the reference dose that has 100% bioavailability

FD_{50} : the dose achieving half maximal reduction in bioavailability

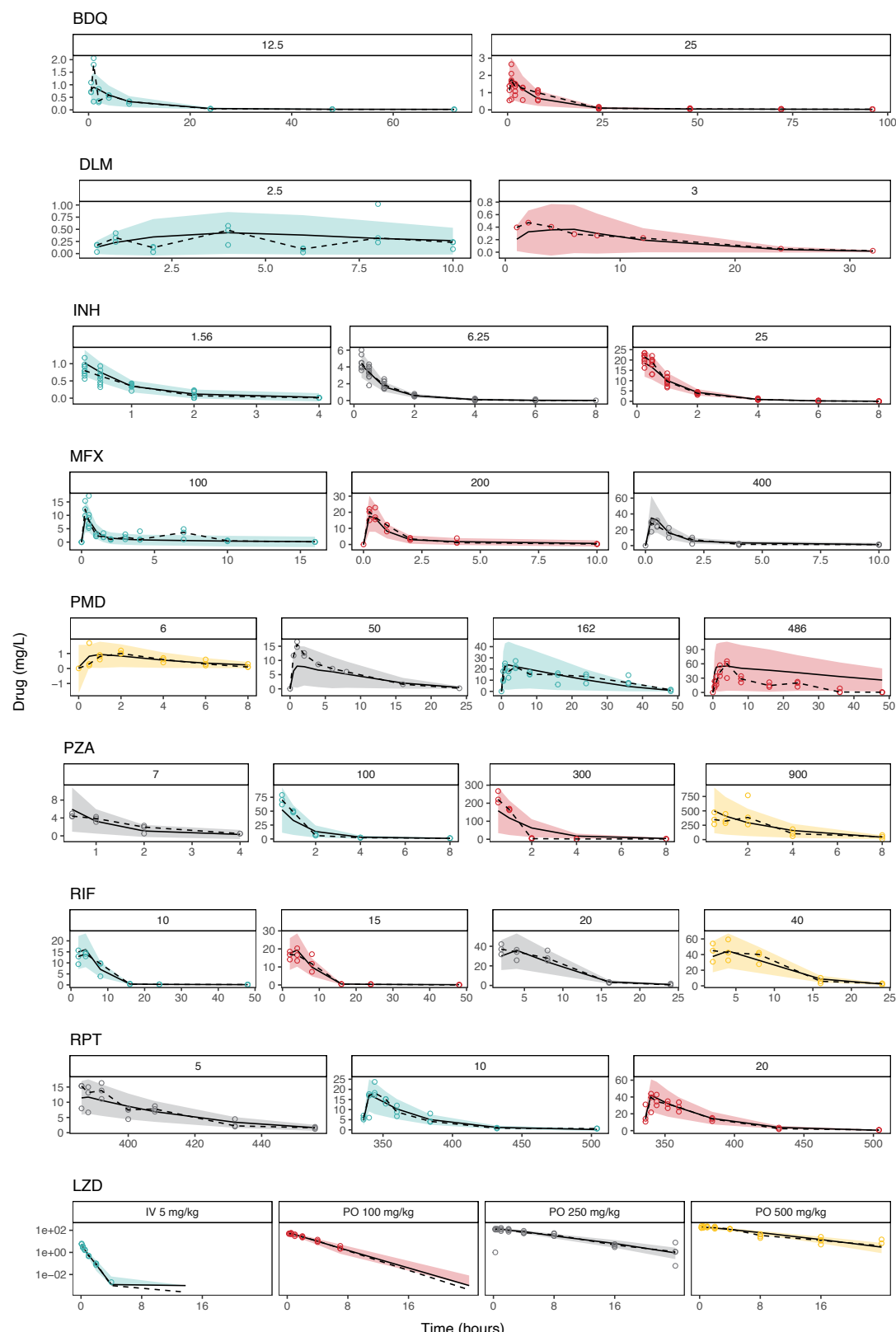


Figure S1 Visual predictive checks for final mouse PK models at representative doses.
All doses are in mg/kg and orally administered unless otherwise stated

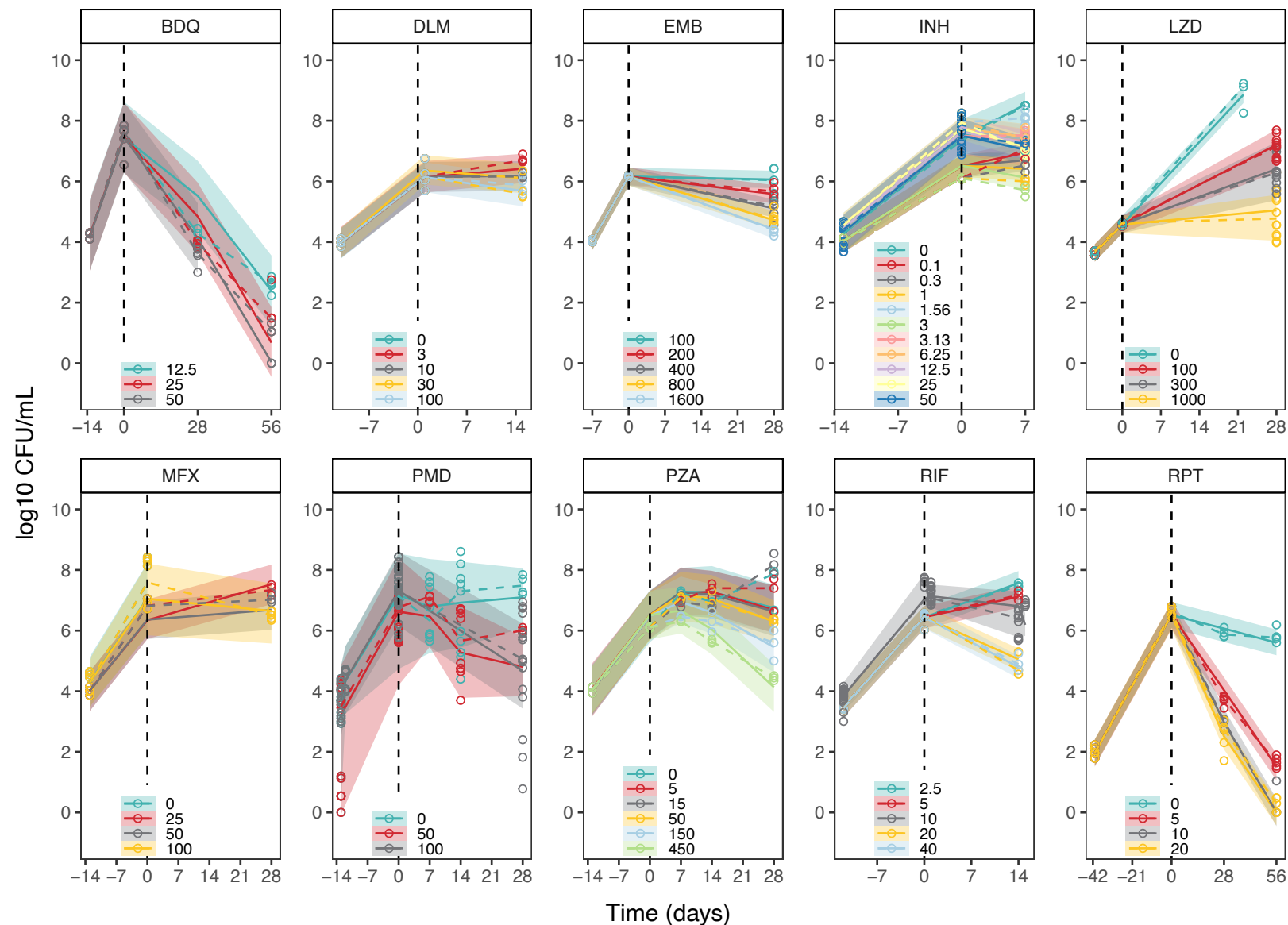


Figure S2 Visual predictive checks for final mouse PD models at representative doses. All doses are in mg/kg and orally administered.

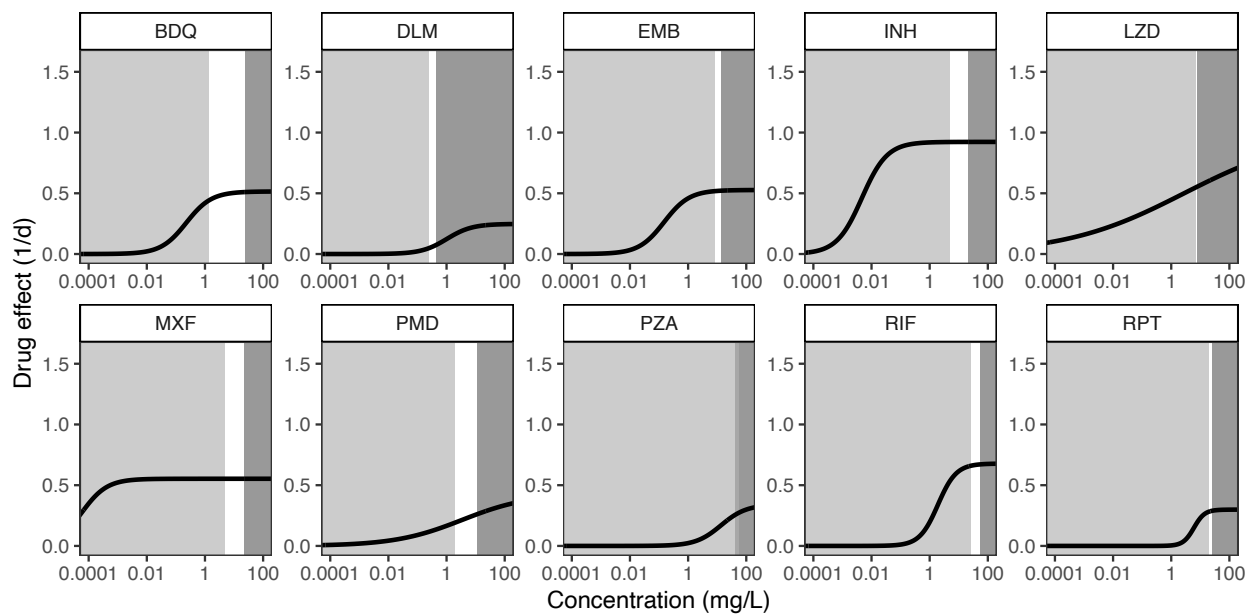


Figure S3 Comparison between human PK concentrations reached at clinical dose levels (light grey), upper limits of drug concentrations within safety ranges (dark grey) and concentration-response relationships for ten TB drugs. Upper limits of clinical dose levels were defined as concentrations up to the C_{\max} . Lower limits of safety ranges were defined as the C_{\max} of the maximum tolerated dose tested in humans.

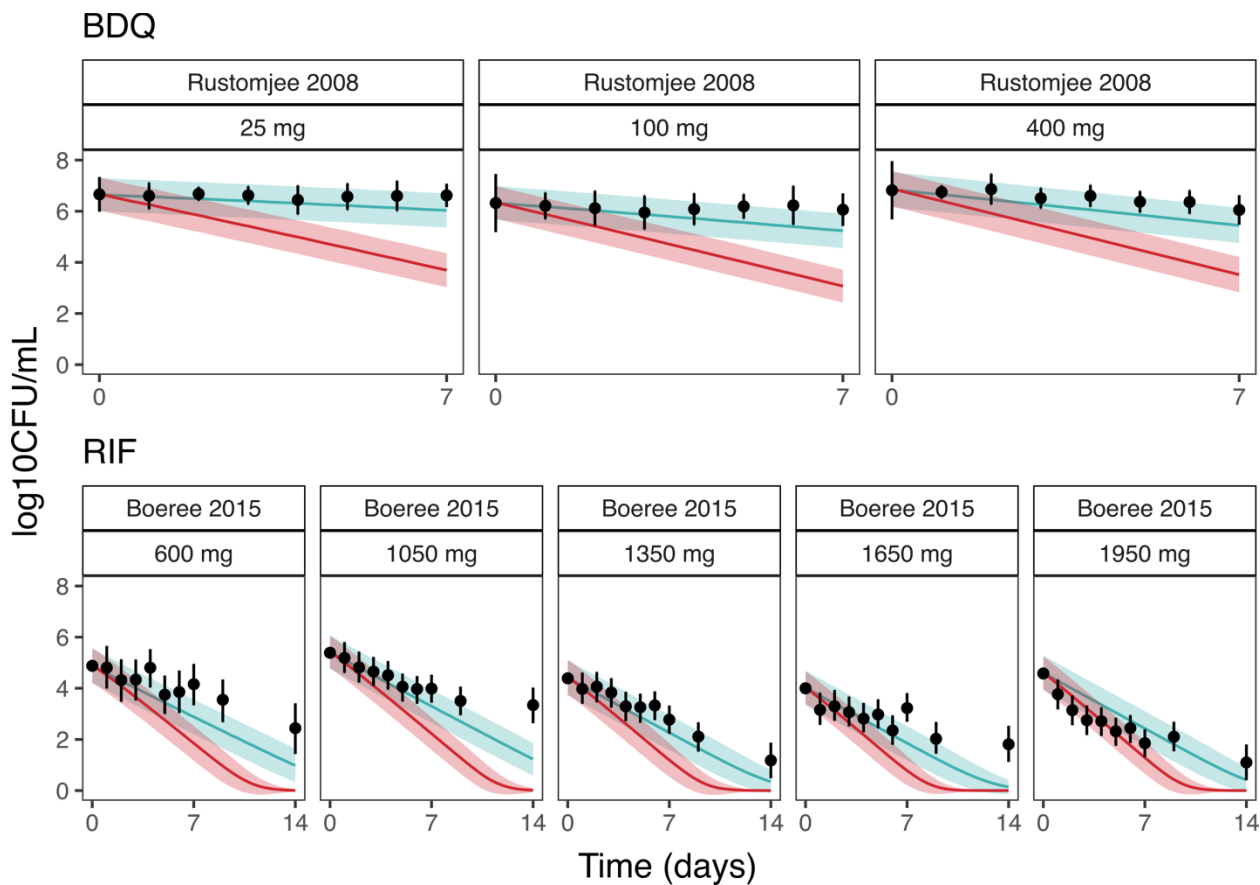


Figure S4 The immune component of the model-based translational platform is essential for accurate prediction of early bactericidal activity. Comparison of prediction of sputum CFU counts in TB patients during treatment with bedaquiline (BDQ) and rifampin (RIF) at multiple dose levels using PKPD relationships from mathematical models when immune effect (imm) is accounted for and not accounted for.

Table S1 Mouse and human PK and PD database of ten TB drugs.

	Mouse PK									
PK data	BDQ	DLM	EMB	INH	LZD	MXF	PMD	PZA	RIF	RPT
Observations	90	29	186	153	238	74	215	100	66	69
Doses (mg/kg)	12.5, 25, single dose	2.5, 3 single dose	10, 16, 30, 100, 300, 1000 mg/kg	1.56, 6.25, 25, single dose	3*, 5*, 100, 250, 500 single dose	100, 200, 400 daily for 32 days	6, 9, 12, 18, 28.8, 50, 54, 162, 486 single dose; 100 daily for 4 or 8 weeks	7, 22, 100, 300, 600, 900, single dose	10, 15, 20, 40, daily for 2 weeks	5, 10, 20, daily for 16 days
Data Source	JHU ⁴	JHU ⁵ and published data ³	Published data ¹	JHU ⁶⁻⁹	JHU ⁷ & TBA	JHU ⁸	JHU ⁵	JHU ^{4,9}	JHU ^{7,9,10}	JHU ¹⁰
Protein binding(f _u , Human/Mouse)	1.0 ¹¹	1.0 ¹²	1.0*	1.455 ^{13,14}	0.986 ^{15,16}	0.797 ¹⁷	0.99 ¹⁸	0.925 ¹⁹ (mouse data JHU unpublished)	4.545 ^{13,20}	0.422 ^{21,22}

*personal communication

	Mouse PD										
PD data	BDQ	DLM	EMB	INH	LZD	MXF	PMD	PZA	RIF	RPT	
Animal	Mouse	Mouse	Mouse	Mouse	Mouse	Mouse	Mouse	Mouse	Mouse	Mouse	
Observations	57	56	54	414	261	63	283	84	203	75	
Doses (mg/kg)	12.5, 25, 50	3, 10, 30, 100	100, 200, 400, 800, 1600	1.0, 3, 1, 3.13, 6.25, 10, 12.5, 25, 30, 50, 100	7.2, 10, 20, 21.4, 30, 40, 60, 72, 100, 200, 300, 335, 1000			3, 5, 10, 15, 25, 30, 37.5,	2.5, 5, 10, 20,		
Treatment duration (days)	70	56	28	21-56	28	28-56	14-28	28-56	14-56	56	

Data Source	JHU ⁴	JHU ⁵ and published data ³	JHU	JHU ⁶⁻⁹	JHU ⁷ & TBA	JHU ⁸	JHU ⁵	JHU ^{4,9}	JHU ^{7,9,10}	JHU ¹⁰
Human PK										
Drugs	PK Structure Model				Doses				No. of Patients / Samples	References
BDQ	3-cmt model with transit absorption				400 mg p.o. daily for 14 days and 200 mg p.o. three times per week for 24 weeks				335 / 2,843	²³
DLM	2-cmt with linear absorption and saturable bioavailability				100, 200, 300, 400 mg p.o. daily for 14 days				744 / 20,483	²⁴
EMB	2-cmt with transit absorption and clearance				800, 1000, 1200, 1500 mg p.o. 5 days/week for ≥ 4 weeks				189 / 1,869	²⁵
INH	2-cmt PK model with linear absorption and clearance				100, 225, 240, 300 and 400 mg p.o. daily, 5 days/week for 2 weeks; 200, 300 and 450 mg p.o. daily, 7 days/week for 1 week				235 / 2,352	²⁶
LZD	2-cmt with non-linear clearance				300 mg, 600 mg or 1200 mg p.o. for 6 months				104 / 497	²⁷
MXF	2-cmt with transit absorption and linear clearance				400 mg p.o. daily for 7 days				241 / 856	²⁸
PMD	1-cmt model with transit absorption and dose-dependent absorption, bioavailability, and volume				200, 600, 1000, 1200 mg p.o. daily for 14 days				1,054 / 17,725	²⁹
PZA	1-cmt PK model with first order absorption and clearance				1200, 1500 and 2000 mg p.o. daily, 5 days/week for 2 weeks; 1000, 1500 and 2000 mg p.o. daily 7 days/week for 2 months				227 / 3,092	³⁰
RIF	1-cmt PK model (saturable bioavailability and elimination, transit absorption and auto-induction)				10, 20, 25, 30, 35, or 40 mg/kg p.o. daily over 2 weeks				83 / 913	³¹

RPT	1-cmt PK model (saturable bioavailability, transit absorption and auto-induction)	300, 450, 600, 750, 900, 1050, 1200, 1350, 1500, 1650, 1800 mg p.o. once weekly up to twice daily for up to four months	863 / 4,388	32
Human EBA studies				
Drugs	Doses	Baseline (\log_{10} CFU/mL)	References	
BDQ	100, 200, 300 and 400 mg (with 200, 400, 500, 700 mg loading dose on first day and 100, 300, 400, 500 mg on second day, respectively)	6.302 (100 mg), 6.001 (200 mg), 6.071 (300 mg), 6.625 (400 mg)		33,34
	25, 100, 400 mg	6.66 (25 mg), 6.32 (100 mg), 6.82 (400 mg)		
DLM	100, 200, 300 and 400 mg	7.06 (100 mg), 6.75 (200 mg), 6.72 (300 mg), 6.82 (400 mg)		35
EMB	15, 25, and 50 mg/kg	6.92		36
INH	9, 18.75, 37.5, 75, 150, 300 and 600 mg	6.491 (9 mg), 6.585 (18.75 mg), 7.169 (37.5 mg), 7.031 (75 mg), 7.115 (150 mg), 6.504 (300 mg), 6.995 (600 mg)		37
LZD	600 mg QD, 600 mg BD	6.34 (600 mg QD), 6.44 (600 mg BD)		38
MXF	400 mg	6.19 (400 mg Johnson), 7.15 (400 mg Pletz), 7.23 (400 mg Gosling)		39-41
PMD	50, 100, 150, 200, 600, 1000, 1200 mg	6.1 (50 mg), 5.8 (100 mg), 6 (150 mg), 6.1 (200 mg Diacon 2012), 6.592 (200 mg Diacon 2010), 6.335 (600 mg), 6.309 (1000 mg), 6.057 (1200 mg)		42,43
PZA	1500, 2000 mg	5.56 (1500mg), 6.910 (2000mg)		36,44
RIF	10, 20, 25, 30 and 35 mg/kg	4.88 (10 mg/kg), 4.00 (20 mg/kg), 5.39 (25 mg/kg), 4.58 (30 mg/kg), 4.39 (35 mg/kg)		20
RPT	300, 600, 900, 1200 mg	N/A		45

*intravenous dosing

Table S2 Final parameters for the bacterial infection model⁴⁶ for each drug based on the control data.

Parameter	BDQ	DLM	EMB	INH	LZD	MXF	PMD	PZA	RIF	RPT
K _g (day ⁻¹) (≤ 4 days)	0.509	0.370	1.11	0.512	0.845	0.461	0.423	0.512	0.512	0.509
K _g (day ⁻¹) (> 4 days)	1.2	0.88104	1.11	1.2168	1.50968	1.1055	1.1935	1.2168	1.2168	1.11
K _d (day ⁻¹)	0.41	0.41	0.41	0.41	0.41	0.41	0.41	0.41	0.41	0.41
K _B (%)	23.695	28.511	20.3	24.174	39	27.478	68.937	24.174	24.174	23.695
B ₅₀ (log ₁₀ CFU)	6.9914	7.0241	7.86	7.0512	8.3385	6.9136	7.7610	7.0512	7.0512	6.9914
γ _B	2.3276	1.2316	0.203	2.1939	2.9	1.7883	0.20574	2.1939	2.1939	2.3276
K _T (%)	66.4	64.722	70.2	66.319	69.6	65.15	63.763	66.319	66.319	66.4
T ₅₀ (day)	19.308	19.725	17.4	19.33	17.5	19.602	18.816	19.33	19.33	19.308
γ _T	5.5277	5.7879	0.702	5.3599	5.13	5.5605	5.7651	5.3599	5.3599	5.5277

B₅₀ = CFU counts to reach half of K_B, BDQ = bedaquiline, CFU = colony forming units, DLM = delamanid, EMB = ethambutol, INH = isoniazid, K_g = bacterial growth rate, K_d = bacterial death rate, KB = bacterial inhibitory CFU-dependent adaptive immune effect, K_T = bacterial inhibitory time-dependent adaptive immune effect, LZD = linezolid, MXF = moxifloxacin, PMD = pretomanid, PZA = pyrazinamide, RIF = rifampin, RPT = rifapentine, T₅₀ = time to reach half of maximal time covariate, γ_B = steepness of the CFU-dependent adaptive immune effect curve, γ_T = steepness of the CFU-dependent adaptive immune effect curve

References

1. Chen, C., Ortega, F., Alameda, L., Ferrer, S. & Simonsson, U. S. H. Population pharmacokinetics, optimised design and sample size determination for rifampicin, isoniazid, ethambutol and pyrazinamide in the mouse. *Eur. J. Pharm. Sci.* **93**, 319–333 (2016).
2. Zhang, N. *et al.* Mechanistic Modeling of *Mycobacterium tuberculosis* Infection in Murine Models for Drug and Vaccine Efficacy Studies. *Antimicrob. Agents Chemother.* **64**, (2020).
3. Sasahara, K. *et al.* Pharmacokinetics and Metabolism of Delamanid, a Novel Anti-Tuberculosis Drug, in Animals and Humans: Importance of Albumin Metabolism In Vivo. *Drug Metab. Dispos.* **43**, 1267–1276 (2015).
4. Irwin, S. M. *et al.* Bedaquiline and Pyrazinamide Treatment Responses Are Affected by Pulmonary Lesion Heterogeneity in *Mycobacterium tuberculosis* Infected C3HeB/FeJ Mice. *ACS Infect Dis* **2**, 251–267 (2016).
5. Tasneen, R. *et al.* Contribution of the nitroimidazoles PA-824 and TBA-354 to the activity of novel regimens in murine models of tuberculosis. *Antimicrob. Agents Chemother.* **59**, 129–135 (2015).
6. Tyagi, S. *et al.* Bactericidal activity of the nitroimidazopyran PA-824 in a murine model of tuberculosis. *Antimicrob. Agents Chemother.* **49**, 2289–2293 (2005).
7. Bigelow, K. M. *et al.* Pharmacodynamic Correlates of Linezolid Activity and Toxicity in Murine Models of Tuberculosis. *J. Infect. Dis.* **223**, 1855–1864 (2021).
8. Yoshimatsu, T. *et al.* Bactericidal activity of increasing daily and weekly doses of moxifloxacin in murine tuberculosis. *Antimicrob. Agents Chemother.* **46**, 1875–1879 (2002).

9. Almeida, D. *et al.* Paradoxical effect of isoniazid on the activity of rifampin-pyrazinamide combination in a mouse model of tuberculosis. *Antimicrob. Agents Chemother.* **53**, 4178–4184 (2009).
10. Rosenthal, I. M. *et al.* Daily dosing of rifapentine cures tuberculosis in three months or less in the murine model. *PLoS Med.* **4**, e344 (2007).
11. Committee for Medicinal Products for Human Use (CHMP). *CHMP assessment report SIRTURO*. https://www.ema.europa.eu/en/documents/variation-report/sirturo-h-c-2614-ii-0033-g-epar-assessment-report_en.pdf (2019).
12. Shimokawa, Y. *et al.* Metabolic Mechanism of Delamanid, a New Anti-Tuberculosis Drug, in Human Plasma. *Drug Metab. Dispos.* **43**, 1277–1283 (2015).
13. Woo, J. *et al.* In vitro protein binding characteristics of isoniazid, rifampicin, and pyrazinamide to whole plasma, albumin, and alpha-1-acid glycoprotein. *Clin. Biochem.* **29**, 175–177 (1996).
14. Jayaram, R. *et al.* Isoniazid pharmacokinetics-pharmacodynamics in an aerosol infection model of tuberculosis. *Antimicrob. Agents Chemother.* **48**, 2951–2957 (2004).
15. Lepak, A. J., Marchillo, K., Pichereau, S., Craig, W. A. & Andes, D. R. Comparative pharmacodynamics of the new oxazolidinone tedizolid phosphate and linezolid in a neutropenic murine *Staphylococcus aureus* pneumonia model. *Antimicrob. Agents Chemother.* **56**, 5916–5922 (2012).
16. Dryden, M. S. Linezolid pharmacokinetics and pharmacodynamics in clinical treatment. *J. Antimicrob. Chemother.* **66**, iv7–iv15 (2011).

17. Siefert, H. M. *et al.* Pharmacokinetics of the 8-methoxyquinolone, moxifloxacin: a comparison in humans and other mammalian species. *J. Antimicrob. Chemother.* **43 Suppl B**, 69–76 (1999).
18. Rakesh *et al.* Synthesis and evaluation of pretomanid (PA-824) oxazolidinone hybrids. *Bioorg. Med. Chem. Lett.* **26**, 388–391 (2016).
19. Stada Pharmaceuticals, Inc, Cranbury, NJ, 2004. Product Information: pyrazinamide oral tablets, pyrazinamide oral tablets. Preprint at
https://www.micromedexsolutions.com/micromedex2/librarian/CS/E2AC9E/ND_PR/evidenceexpert/ND_P/evidenceexpert/DUPLICATIONSHIELDSYNC/C17097/ND_PG/evidenceexpert/ND_B/evidenceexpert/ND_AppProduct/evidenceexpert/ND_T/evidenceexpert/PFACTIONID/evidenceexpert.DoIntegratedSearch?SearchTerm=pyrazinamide&UserSearchTerm=pyrazinamide&SearchFilter=filterNone&navitem=searchALL#cite5_dp.
20. de Steenwinkel, J. E. M. *et al.* Optimization of the rifampin dosage to improve the therapeutic efficacy in tuberculosis treatment using a murine model. *Am. J. Respir. Crit. Care Med.* **187**, 1127–1134 (2013).
21. sanofi-aventis U.S. (per manufacturer), Bridgewater, NJ, 2014. Product Information: PRIFTIN(R) oral tablets, rifapentine oral tablets. Preprint at
https://www.micromedexsolutions.com/micromedex2/librarian/CS/A32D19/ND_PR/evidenceexpert/ND_P/evidenceexpert/DUPLICATIONSHIELDSYNC/0EBD73/ND_PG/evidenceexpert/ND_B/evidenceexpert/ND_AppProduct/evidenceexpert/ND_T/evidenceexpert/PFACTIONID/evidenceexpert.DoIntegratedSearch?SearchTerm=rifapentine&UserSearchTerm=rifapentine&SearchFilter=filterNone&navitem=searchALL#cite2_dp.

22. Assandri, A., Ratti, B. & Cristina, T. Pharmacokinetics of rifapentine, a new long lasting rifamycin, in the rat, the mouse and the rabbit. *J. Antibiot.* **37**, 1066–1075 (1984).
23. Svensson, E. M., Dosne, A.-G. & Karlsson, M. O. Population Pharmacokinetics of Bedaquiline and Metabolite M2 in Patients With Drug-Resistant Tuberculosis: The Effect of Time-Varying Weight and Albumin. *CPT Pharmacometrics Syst Pharmacol* **5**, 682–691 (2016).
24. Wang, X., Mallikaarjun, S. & Gibiansky, E. Population Pharmacokinetic Analysis of Delamanid in Patients with Pulmonary Multidrug-Resistant Tuberculosis. *Antimicrob. Agents Chemother.* **65**, (2020).
25. Jönsson, S. *et al.* Population pharmacokinetics of ethambutol in South African tuberculosis patients. *Antimicrob. Agents Chemother.* **55**, 4230–4237 (2011).
26. Wilkins, J. J. *et al.* Variability in the population pharmacokinetics of isoniazid in South African tuberculosis patients. *Br. J. Clin. Pharmacol.* **72**, 51–62 (2011).
27. Imperial, M. Z., Nedelman, J. R., Conradie, F. & Savic, R. M. Proposed Linezolid Dosing Strategies to Minimize Adverse Events for Treatment of Extensively Drug-Resistant Tuberculosis. *Clin. Infect. Dis.* **74**, 1736–1747 (2021).
28. Zvada, S. P. *et al.* Moxifloxacin population pharmacokinetics and model-based comparison of efficacy between moxifloxacin and ofloxacin in African patients. *Antimicrob. Agents Chemother.* **58**, 503–510 (2014).
29. Salinger David H., Subramoney Vishak, Everitt Daniel & Nedelman Jerry R. Population Pharmacokinetics of the Antituberculosis Agent Pretomanid. *Antimicrob. Agents Chemother.* **63**, e00907-19 (2019).

30. Wilkins, J. J. *et al.* Variability in the population pharmacokinetics of pyrazinamide in South African tuberculosis patients. *Eur. J. Clin. Pharmacol.* **62**, 727–735 (2006).
31. Svensson, R. J. *et al.* A Population Pharmacokinetic Model Incorporating Saturable Pharmacokinetics and Autoinduction for High Rifampicin Doses. *Clin. Pharmacol. Ther.* **103**, 674–683 (2018).
32. Hibma, J. E. *et al.* Rifapentine Population Pharmacokinetics and Dosing Recommendations for Latent Tuberculosis Infection. *Am. J. Respir. Crit. Care Med.* **202**, 866–877 (2020).
33. Diacon, A. H. *et al.* Randomized dose-ranging study of the 14-day early bactericidal activity of bedaquiline (TMC207) in patients with sputum microscopy smear-positive pulmonary tuberculosis. *Antimicrob. Agents Chemother.* **57**, 2199–2203 (2013).
34. Rustomjee, R. *et al.* Early bactericidal activity and pharmacokinetics of the diarylquinoline TMC207 in treatment of pulmonary tuberculosis. *Antimicrob. Agents Chemother.* **52**, 2831–2835 (2008).
35. Diacon, A. H. *et al.* Early bactericidal activity of delamanid (OPC-67683) in smear-positive pulmonary tuberculosis patients. *Int. J. Tuberc. Lung Dis.* **15**, 949–954 (2011).
36. Jindani, A., Aber, V. R., Edwards, E. A. & Mitchison, D. A. The early bactericidal activity of drugs in patients with pulmonary tuberculosis. *Am. Rev. Respir. Dis.* **121**, 939–949 (1980).
37. Donald, P. R. *et al.* The early bactericidal activity of isoniazid related to its dose size in pulmonary tuberculosis. *Am. J. Respir. Crit. Care Med.* **156**, 895–900 (1997).
38. Dietze, R. *et al.* Early and extended early bactericidal activity of linezolid in pulmonary tuberculosis. *Am. J. Respir. Crit. Care Med.* **178**, 1180–1185 (2008).

39. Gosling, R. D. *et al.* The bactericidal activity of moxifloxacin in patients with pulmonary tuberculosis. *Am. J. Respir. Crit. Care Med.* **168**, 1342–1345 (2003).
40. Johnson, J. L. *et al.* Early and extended early bactericidal activity of levofloxacin, gatifloxacin and moxifloxacin in pulmonary tuberculosis. *Int. J. Tuberc. Lung Dis.* **10**, 605–612 (2006).
41. Pletz, M. W. R. *et al.* Early bactericidal activity of moxifloxacin in treatment of pulmonary tuberculosis: a prospective, randomized study. *Antimicrob. Agents Chemother.* **48**, 780–782 (2004).
42. Diacon, A. H. *et al.* Early bactericidal activity and pharmacokinetics of PA-824 in smear-positive tuberculosis patients. *Antimicrob. Agents Chemother.* **54**, 3402–3407 (2010).
43. Diacon, A. H. *et al.* Phase II dose-ranging trial of the early bactericidal activity of PA-824. *Antimicrob. Agents Chemother.* **56**, 3027–3031 (2012).
44. Diacon, A. H. *et al.* Bactericidal activity of pyrazinamide and clofazimine alone and in combinations with pretomanid and bedaquiline. *Am. J. Respir. Crit. Care Med.* **191**, 943–953 (2015).
45. Sirgel, F. A. *et al.* The early bactericidal activities of rifampin and rifapentine in pulmonary tuberculosis. *Am. J. Respir. Crit. Care Med.* **172**, 128–135 (2005).
46. Zhang Nan *et al.* Mechanistic Modeling of Mycobacterium tuberculosis Infection in Murine Models for Drug and Vaccine Efficacy Studies. *Antimicrob. Agents Chemother.* **64**, e01727-19 (2020).